Petrography, mineralogy, and trace element geochemistry of lunar meteorite Dhofar 1180

Aicheng ZHANG^{1, 2} and Weibiao HSU^{3*}

¹Laboratory for Astrochemistry and Planetary Sciences, Lunar and Planetary Science Center, Purple Mountain Observatory, Chinese Academy of Sciences, 2 West Beijing Road, Nanjing, 210008, China
²State Key Laboratory for Mineral Deposits Research, Nanjing University, Nanjing 210093, China
³Faculty of Earth Science, China University of Geosciences, Wuhan 430074, China
*Corresponding author. E-mail: wbxu@pmo.ac.cn

(Received 06 August 2008; revision accepted 19 February 2009)

Abstract—Here we report the petrography, mineralogy, and trace element geochemistry of the Dhofar 1180 lunar meteorite. Dhofar 1180 is predominantly composed of fine-grained matrix with abundant mineral fragments and a few lithic and glassy clasts. Lithic clasts show a variety of textures including cataclastic, gabbroic, granulitic, ophitic/subophitic, and microporphyritic. Both feldspathic and mafic lithic clasts are present. Most feldspathic lithic clasts have a strong affinity to ferroan anorthositic suite rocks and one to magnesian suite rocks. Mafic lithic clasts are moderately to extremely Fe-rich. The Ti/[Ti+Cr]-Fe/[Fe+Mg] compositional trend of pyroxenes in mafic lithic clasts is consistent with that of low-Ti mare basalts. Glasses display a wide chemical variation from mafic to feldspathic. Some glasses are very similar to those from Apollo 16 soils. KREEP components are essentially absent in Dhofar 1180. One glassy clast is rich in K, REE and P, but its Mg/[Mg+Fe] is very low (0.25). It is probably a last-stage differentiation product of mare basalt. Molar Fe/Mn ratios of both olivine and pyroxene are essentially consistent with a lunar origin.

Dhofar 1180 has a LREE-enriched (La $18 \times CI$, Sm $14 \times CI$) pattern with a small positive Eu anomaly (Eu $15 \times CI$). Th concentration is 0.7 ppm in Dhofar 1180. Petrography, mineralogy, and trace element geochemistry of Dhofar 1180 are different from those of other lunar meteorites, indicating that Dhofar 1180 represents a unique mingled lunar breccia derived from an area on the lunar nearside but far away from the center of the Imbrium Basin.

INTRODUCTION

Lunar rocks and soils are important samples to understand the chemical composition and magmatic evolution of the Moon. In the past 40 years, Apollo and Luna samples played a predominant role on establishing formation and evolution models of the Moon (e.g., magma ocean model of lunar evolution, Warren 1985). However, these lunar samples were collected from a limited area (only 5-8% of the lunar surface) on the nearside of the Moon (Warren and Kallemeyn 1991). This area was later found to be geochemically anomalous based on Clementine and Lunar Prospector data and defined as Procellarum KREEP Terrane (PKT) (Jolliff et al. 2000). On the other hand, lunar meteorites represent random samples ejected from the Moon, very likely from regions not sampled by the Apollo and Luna missions (Korotev 2005). They provide an important complementary source of data for understanding the nature and evolutionary history of the lunar

crust. For instance, some meteorites that were probably derived from the far side of the Moon could provide clues to understand global distribution of rock types (Takeda et al. 2006; Hsu et al. 2008). Up to date, more than 60 unpaired lunar meteorites have been recovered from hot and cold deserts (Korotev et al. 2008). Based on bulk Al₂O₃ content, these lunar meteorites could be divided into three groups: mare basalts and breccias with low Al₂O₃ contents (8–10 wt%), feldspathic breccias with high Al₂O₃ contents (26–31 wt%), and mingled breccias containing both basaltic and feldspathic components with intermediate Al₂O₃ contents (10-26 wt%) to mare basalts and feldspathic breccias (Korotev 2005). Most lunar meteorites, except SaU 169 (Gnos et al. 2004; Al-Kathiri et al. 2007), Northwest Africa (NWA) 4472 (Joy et al. 2007), and Calcalong Creek (Hill and Boynton 2003), contain negligible amount of KREEP component which is rich in potassium (K), rare-earth-elements (REE), phosphorus (P), and other incompatible trace elements.

In the Dhofar region of Oman, more than 1000 meteorites have been discovered, including about 50 lunar meteorites. Most lunar meteorites found in the Dhofar region are feldspathic breccias with high bulk Al₂O₃ (>26 wt%). Dhofar 1180 is one of the three non-feldspathic breccias (Dhofar 287, Dhofar 925/969/961, and Dhofar 1180). It weighs 115.2 gram and has a shape like a thick-bladed talon. Bunch et al. (2006) reported that Dhofar 1180 contains 22.6 wt% Al₂O₃, 9.3 wt% FeO, and 0.9 ppm Th, similar in composition to Calcalong Creek and Yamato (Y-) 983885 except a lower bulk Mg/Fe ratio and lower concentrations of incompatible trace elements. Dhofar 1180 is one of the most Al₂O₃-rich samples among the mingled breccias (Korotev et al. 2008). In this paper, we report detailed petrography, mineralogy, and trace element geochemistry of Dhofar 1180, discuss its lunar origin, and make a comparison with other lunar samples. Some preliminary results of this study were reported elsewhere (Zhang and Hsu 2006, 2007).

ANALYTICAL METHODS

A slice of Dhofar 1180 (0.33 g) was acquired from Michael Farmer, the holder of the main mass. Two polished thin sections (PMO-1027 and PMO-1028) were made and examined with an optical microscope and a Hitachi S-3400N scanning electron microscope (SEM). Mineral modal abundances of lithic clasts were determined backscattered electron (BSE) images with Adobe Photoshop software. Mineral chemistry was analyzed with electron microprobes (EMP) at Nanjing University (JEOL JXA-8800M) and at Chinese University of Geosciences (JEOL 8100). The operating conditions are 15–20 keV accelerating voltage, 20 nA beam current, and a focused beam. Natural and synthetic standards were used: plagioclase (Na, Al), Kfeldspar (K), Cr₂O₃ (Cr), diopside (Ca, Mg, Si), MnSiO₃ (Mn), hornblende and andradite (Fe in silicate and oxide phases), and metal Fe (Fe in metal and sulfide), rutile (Ti), apatite (P), metal (Ni), chalcopyrite (S), metal Co (Co), and synthetic phosphate glasses for La, Ce, Th, and Y. All data were reduced by ZAF procedures. Detection limits typically are: Na 110 ppm, K 90 ppm, Mg 100 ppm, Fe 190 ppm, Al 100 ppm, Mn 180 ppm, Si 130 ppm, Cr 130 ppm, Ti 210 ppm, Ca 120 ppm, P 85 ppm, La 85 ppm, Th 125 ppm, Y 205 ppm, and Ce 175 ppm.

Trace-element concentrations of 91.19 mg Dhofar 1180 sample were analyzed with instrumental neutron activation analysis (INAA) at Washington University in St. Louis. A 91.19 mg Dhofar 1180 sample was crushed into small fragments (<3 mm) and fit in silica sample tubes. Samples were irradiated for 12 hours in a thermal neutron flux of 5×10^{13} cm⁻² s⁻¹ at the University of Missouri Research Reactor. The sample was analyzed three times, first for about 10–15 minutes between 6 and 7 days following irradiation, second for 1.5–2 hours between 7 and 11 days

following irradiation, and finally for at least three hours sometime after 28 days following the irradiation. The detailed analytical procedures were described by Korotev (1991, 1996).

RESULTS

Petrography

Dhofar 1180 is composed of a few lithic clasts, glasses and abundant mineral fragments that set in a fine-grained matrix (Fig. 1). The lithic clasts, glasses, and mineral fragments show irregular shapes and variable sizes (from $\sim 10~\mu m$ to $\sim 1.5~mm$ across) and textures (Figs. 2–6). The matrix is made up of fine-grained minerals bound by dark glassy cement. No fusion crust, glassy spheres, and melt veins were observed in the two thin sections.

Lithic clasts in Dhofar 1180 show a large variation in texture and modal abundance of constituent minerals (Figs. 2–3 and Table 1). Lithic clasts C-4, C-5, C-7, C-9, C-12, C-13, and C-14 have high modal abundance of plagioclase (>60 area%). They are feldspathic clasts and display granulitic, ophitic, and microporphyritic textures (Fig. 2). In most of these clasts, olivine and pyroxene are fine-grained (<20 μ m) and generally homogeneous in composition. Lithic clast C-8 has high abundance of olivine (42 area%) and relatively low abundance of plagioclase (52 area%). However, because this clast consists of very coarse-grained (~300 μ m) olivine and plagioclase relative to the small size (500 μ m) of the clast, the modal abundance may not be representative.

Dhofar 1180 also contains a few lithic clasts (C-1, C-2, C-3, C-6, C-10, C-11, and C-15) that consist dominantly of mafic materials (Table 1). C-1 has a cataclastic texture (Fig. 2a) and contains ulvöspinel, zoned pyroxene, and pyroxferroite grains, indicating a degraded basaltic breccia. C-2 has a typical basaltic texture (Fig. 2b) with pyroxene grains showing chemical zoning. Pyroxferroite occurs as rims of pyroxene grains. In this clast, Si,K-rich glass and Ca,Al-rich glass occur in the interstice between pyroxene and plagioclase grains and show an immiscible texture (Fig. 2c). These glasses are crosscut by elongated ilmenite crystals. Lithic clast C-3 contains plagioclase, augite and pigeonite with exsolution lamellae (lamella width <1 µm), olivine, ulvöspinel, and ilmenite. The occurrence of ulvöspinel and ilmenite suggests this clast is basaltic, although it has an apparently high modal abundance of plagioclase (~65 area%). C-6 contains some porphyritic grains of olivine and pyroxene and the groundmass exhibits a subophitic texture. In this clast, pigeonite grains exhibit exsolution lamellae of augite (from submicron to ~2 µm) (Fig. 2h). Two grains of chromiteulvöspinel-hercynite solid solution also exist in this clast. Minerals in C-10 are very fine-grained (<15 µm) with olivine, pigeonite, and ilmenite embraced by plagioclase. In C-11, fayalite, ferroaugite, and silica occur as fine-grained eutectoid

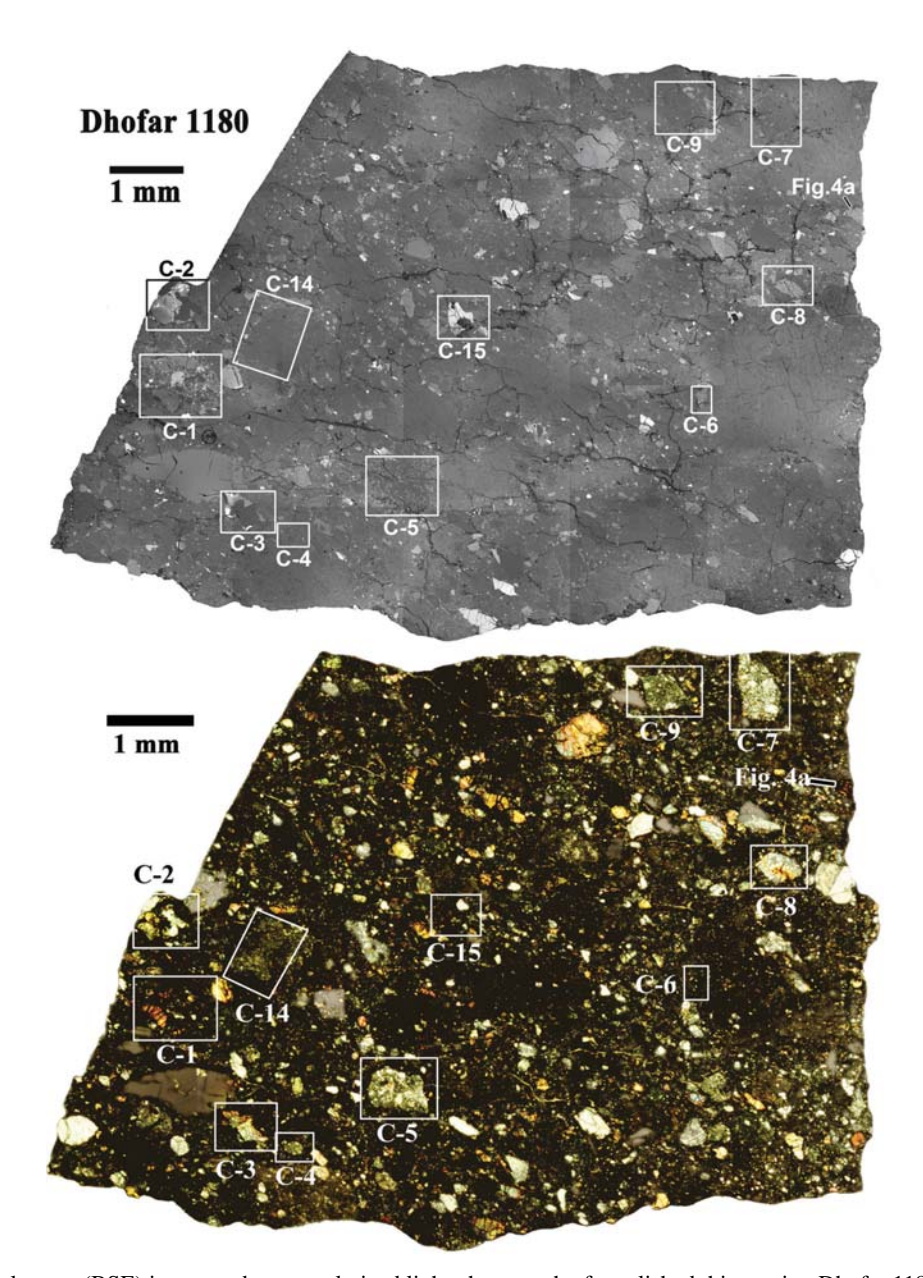


Fig. 1. Backscattered electron (BSE) image and cross-polarized light photograph of a polished thin section Dhofar 1180 (PMO-1027). Lithic clasts, glasses, and mineral fragments are embedded in fine-grained matrix. White rectangular areas correspond to specific lithic clasts that were investigated in detail for their texture and mineralogy and discussed in the text.

assemblage. Fayalite, ferroaugite, and silica form triple junction grain boundary (Fig. 2m). C-15 consists of fayalite, hedenbergite, ilmenite, K-rich feldspar, apatite, merrillite, silica, troilite, and baddeleyite (Fig. 3). Fayalite is dominant (~82 area%) and hedenbergite is subordinate, with K-rich feldspar, silica, apatite, merrillite, troilite, and baddeleyite set in the interstice between fayalite and hedenbergite. K-rich feldspar grains intergrow with thin blades of silica (Fig. 3b). Some anhedral merrillite grains are enclosed by large hedenbergite grains (Fig. 3b).

Glasses in Dhofar 1180 are usually irregular in shape and appear in different sizes (a few tens microns to ~1.5 mm)

(Fig. 4). Only one glass clast has a near-circular shape (Fig. 4b). Most glasses are mafic (MgO+FeO=19.34–40.96 wt%). A few are feldspathic (Al $_2$ O $_3$ =28.95–36.12 wt%), and one glass is mafic and P-rich (up to 6.25 wt% P $_2$ O $_5$). Some mafic glasses contain scattered irregular grains of olivine, pyroxene, and feldspar (Figs. 4a–d). One mafic glass is attached to a large pigeonite grain (Fig. 4c). Feldspathic glasses are homogeneous within an individual glass and some contain relict grains of olivine and pyroxene (Fig. 4f). A few very fine-grained metal grains (<2 μ m) are observed in some mafic glasses (e.g., Figs. 4b and 4d). The feldspathic glass in Fig. 4e shows devitrification at the margin. The P-rich glass is about

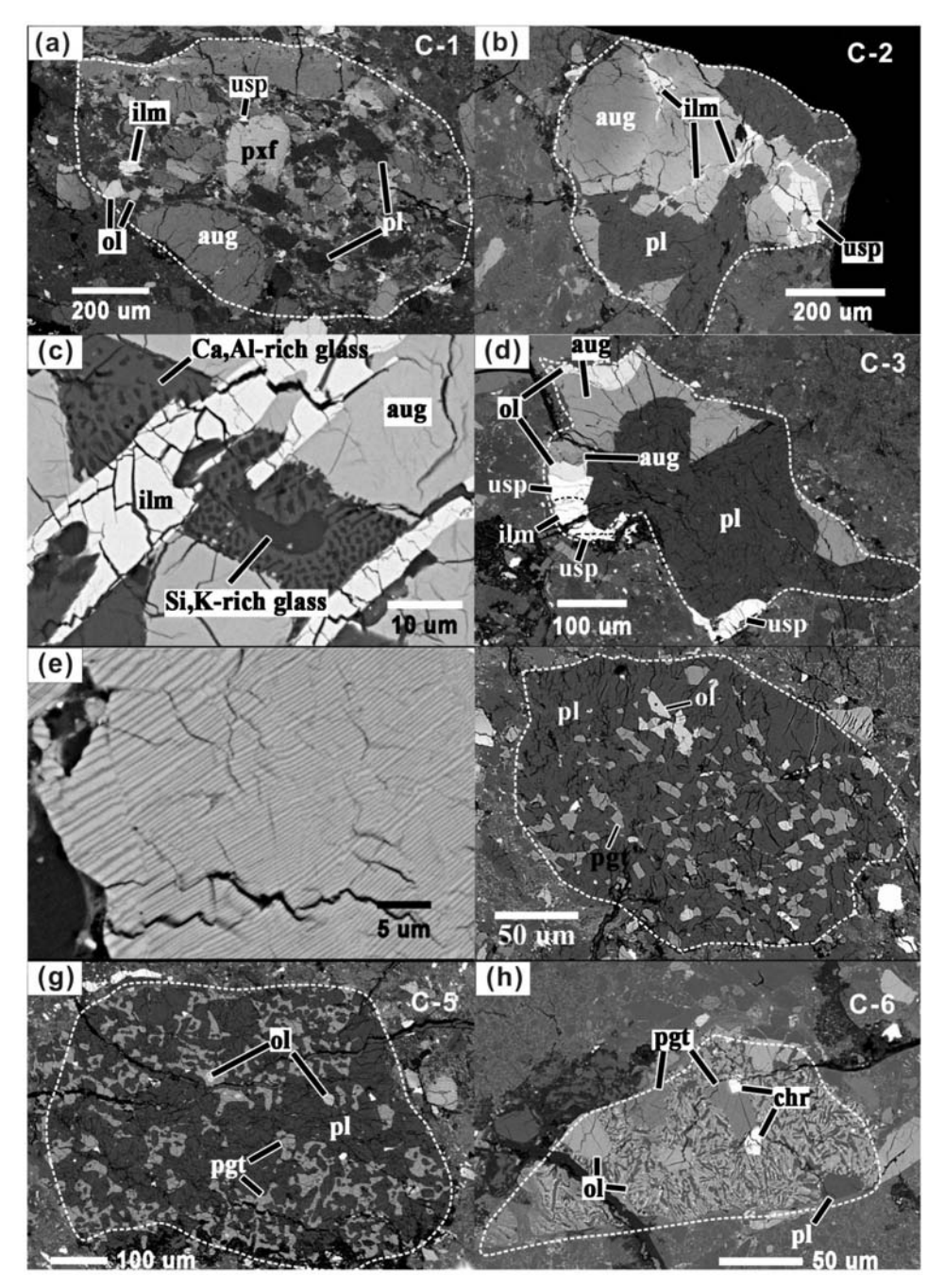


Fig. 2. BSE images of lithic clasts in Dhofar 1180. a) Cataclastic basalt clast containing augite (aug), pyroxferroite (pxf), olivine (ol), plagioclase (pl), and minor ilmenite (ilm) and ulvöspinel (usp). b) Basalt clast containing mainly of zoned pyroxene and plagioclase. Mixtures of Si,K-rich glass and Ca,Al-rich glass occur in the interstices between pyroxene and plagioclase. c) A close-up image of (b). Opaque minerals occur in the interstices of pyroxene grains or crosscut pyroxene and the mixture of Si,K-rich glass and Ca,Al-rich glass. d) A lithic clast containing augite, olivine, ilmenite, and ulvöspinel around plagioclase. e) Some augite grains in (d) show submicron-scaled exsolution lamellae (<1 μm). f) Gabbroic anorthosite clast containing fine-grained pigeonite (pgt) and olivine enclosed by plagioclase. g) Gabbroic anorthosite clast with typical granulitic texture. Some pigeonite grains interconnect each other and include olivine grains. Pyroxene grains show rounded grain boundary. h) A lithic clast with subophitic texture of olivine and plagioclase including olivine, exsolved pyroxene, and chromite-ulvöspinel-spinel grains.

30 µm in its longest dimension (Fig. 5a). On the BSE image, it consists of three portions with different textures: left portion (L), right portion (R) containing some sub-micron spherules, and middle portion (M) with a vermiform mixture

of two immiscible glasses (Fig. 5a). No crystals and devitrification were observed in this glass.

Mineral fragments in the matrix of Dhofar 1180 are mainly olivine, pyroxene, and plagioclase. Fragments of ilmenite,

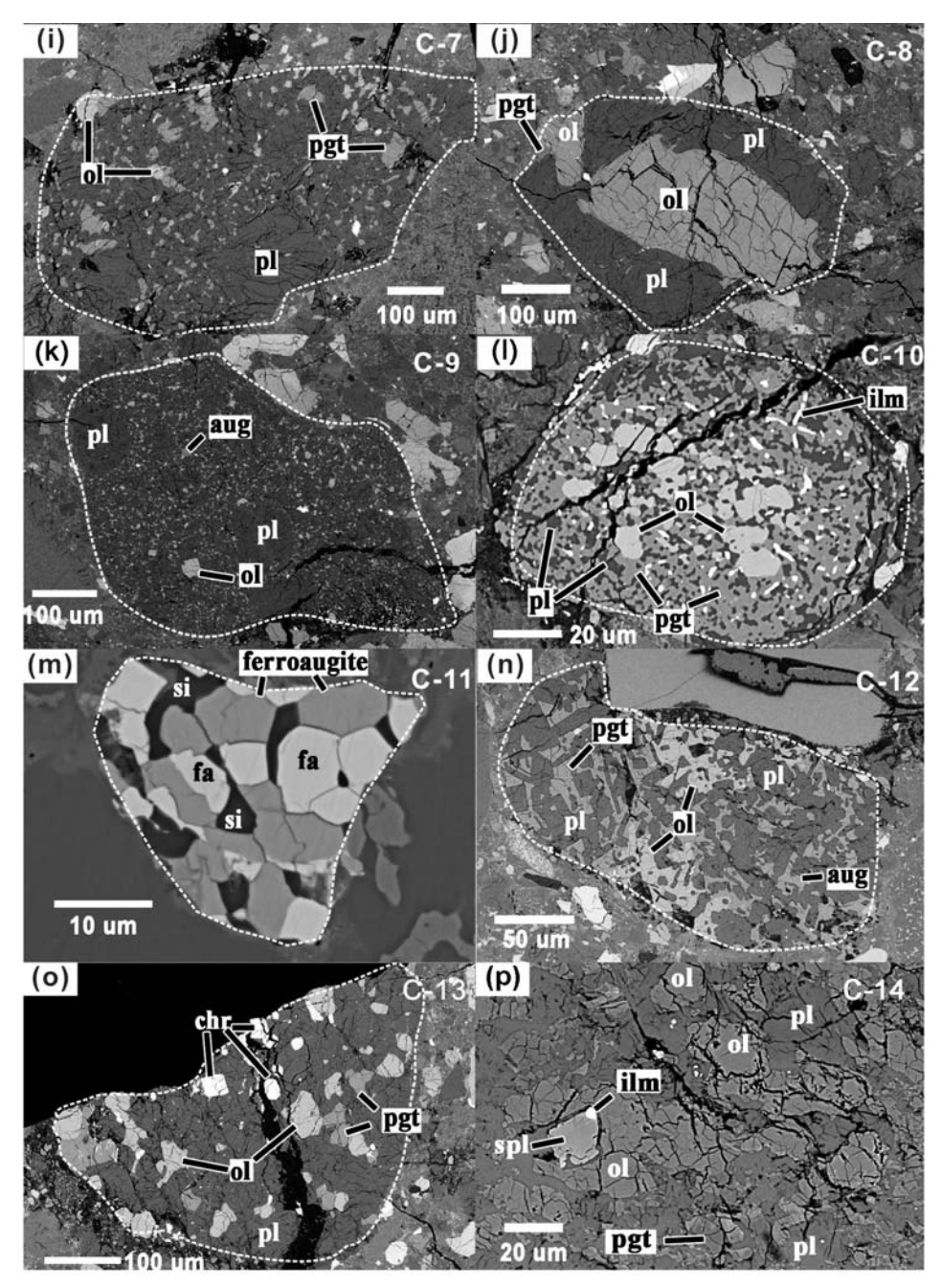


Fig. 2. Continued. i) Gabbroic anorthosite with very-fine-grained to fine-grained pigeonite and olivine grains dispersed in the interstices of plagioclase grains. j) A lithic clast composed of olivine, plagioclase, and pigeonite. k) Anorthosite with microporphyritic texture composed of pyroxene, olivine, and minor opaque minerals. l) A lithic clast composed of fine-grained olivine, pyroxene, plagioclase and ilmenite. m) Ferroaugite-fayalite (fa)-silica (si) assemblage. Ferroaugite, fayalite, and silica show a triple junction grain boundary. n) Olivine anorthositic gabbro with ophitic texture composed of plagioclase, pigeonite, olivine, and minor augite. o) Troctolitic anorthosite composed of plagioclase and subhedral-euhedral grains of olivine, pigeonite, and chromite (chr). p) Part of a spinel anorthositic troctolite containing plagioclase, olivine, and minor pyroxene and spinel (spl). In this clast, olivine and pyroxene typically are heavily fractured.

ulvöspinel-chromite-hercynite solid solution, Fe-Ni metal, and sulfide also exist. Olivine fragments are commonly anhedral to subhedral in shape and vary in size from several microns to about 500 microns. Olivine fragments are homogeneous in composition. Pyroxene fragments are also anhedral to subhedral in shape and have a similar size distribution to that of

olivine fragments. Pyroxene fragments usually show exsolution lamellae on various scales (from <2 μm to up to 9 μm , Figs. 6a, 6b) or core-to-rim chemical zoning. Plagioclase fragments are anhedral to subhedral and have a large variation of size distribution (up to 1.8 mm). Ilmenite grains are anhedral to subhedral and range from 20 to 250 μm in size. Ulvöspinel-

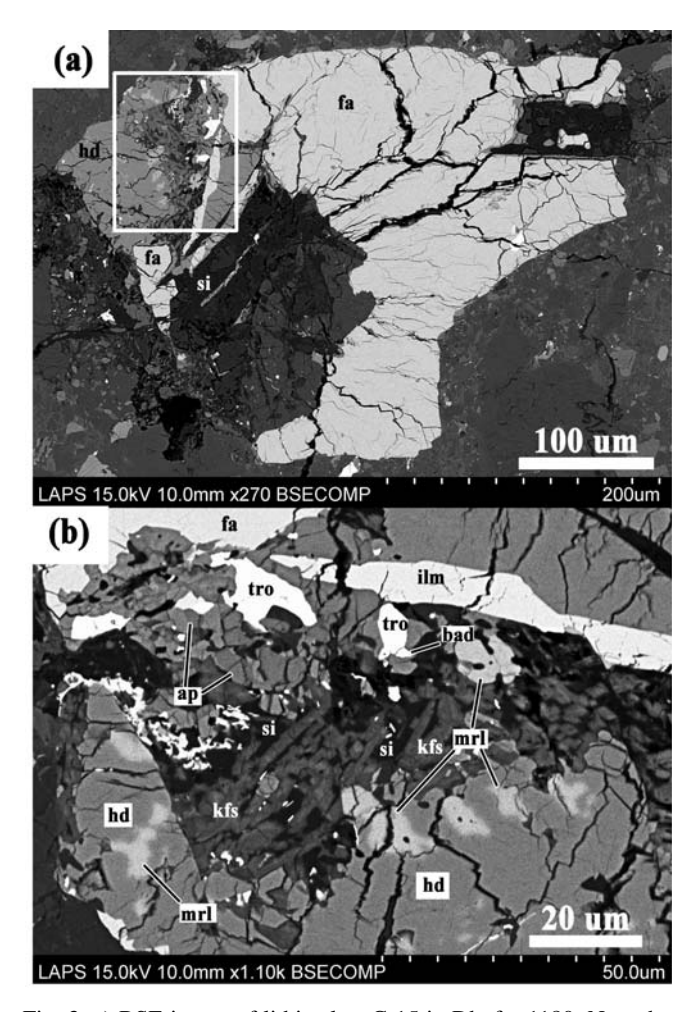


Fig. 3. a) BSE image of lithic clast C-15 in Dhofar 1180. Note that parts of the clast have been altered. b) The mineral assemblage of Krich feldspar (kfs), silica (si), apatite (ap), merrillite (mrl), ilmenite (ilm), troilite (tro), baddeleyite (bad) occurs in the interstice between fayalite (fa) and hedenbergite (hd). Some anhedral merrillite grains are included in hedenbergite.

chromite-hercynite fragments are relatively small (<40 $\mu m)$ and one grain is rimmed with an Al-rich thin rim. Both Fe-Ni metal and sulfide fragments are observed, and sulfide grains are slightly more abundant than Fe-Ni metal. They are usually small in size (<60 μm) and only one fragment is up to 120 μm . Some metal grains are weathered along their rims.

Mineral Chemistry

Representative EMP analyses of lithic and fragment minerals (olivine, pyroxene, plagioclase, oxide minerals, phosphate minerals, Fe-Ni metal, and sulfide) are given in Tables 2–7. In Dhofar 1180, pyroxene compositions display a large variation as shown in pyroxene quadrilateral (Fig. 7). Pyroxene grains in most lithic clasts (C-4, C-5, C-7, C-9, C-12, and C-13) have moderate Mg# (molar Mg/[Mg+Fe]) values (0.64–0.7). Pyroxene grains in C-8 and C-14 are magnesian (Mg#=0.74 and

0.85–0.86, respectively). Pyroxene grains in these lithic clasts are mainly low-Ca pyroxene ($En_{57.8-62.8}Fs_{25.0-37.3}Wo_{516}$). High-Ca pyroxene grains (En_{47,4-50,4}Fs_{21,8-25,1}Wo_{24,5-30,7}) occur in C-9 and C-12. Pigeonite grains in C-14 are the most magnesian (Mg#=0.85-0.86) in Dhofar 1180 and shows a narrow compositional variation (En_{78.2-79.3}Fs_{13.4-13.7}Wo_{7.3-8.1}). Pyroxene grains in C-6 include pigeonite (En_{55.7-57.2}Fs_{35.6-37.3}Wo_{5.5-8.7}) and augite (En_{42.4}Fs_{18.5}Wo_{39.1}) and have moderate Mg# values (0.61-0.7). Pyroxene grains in C-10 are pigeonite (En_{52.2-55.5} $Fs_{33.7\text{--}36.3}Wo_{8.5\text{--}10.4})$ with a limited variation of Mg# (0.6–0.61). Pyroxene grains in other mafic lithic clasts (C-1, C-2, C-3, C-11, and C-15) are Fe-rich and their compositions vary from clast to clast (Fig. 7). Pyroxene grains in C-1 and C-2 show a large compositional variation (En_{0.54-7.6}Fs_{22.8-86} Wo_{13.5-37.9} and $En_{0.44-7.3}Fs_{28.6-79.7}Wo_{12.2-34.7}$, respectively) and are generally Fe-rich (Mg#=0.01-0.63). Pyroxferroite (En_{0.4-2.0}Fs_{75.2-86.0} Wo_{13.5-22.9}) occurs in C-1 and C-2. Augite (En_{30.8} Fs_{34.9}Wo_{34.3}) in C-3 is moderately Fe-rich (Mg#=0.47), but low-Ca pyroxene lamellae are too thin to obtain ideal pigeonite or orthopyroxene composition. Ferroaugite in C-11 has a relatively homogeneous composition $(En_{16.4-17.0}Fs_{46.9-49.0}Wo_{34.4-36.7}, Mg\#=0.25-0.26).$ Hedenbergite in C-15 is extremely Fe-rich (Mg#=0.04-0.06, $En_{2,2-3,3}Fs_{51,4-52,9}Wo_{44,4-45,4}$). Pyroxene fragments have a similar compositional range ($En_{0.87-7.4}$ $Fs_{15.1-81.9}$ $Wo_{1.64-5.6}$, Mg#=0.01-0.8) to those in lithic clasts. Dhofar 1180 pyroxenes commonly contain low Cr₂O₃ and TiO₂ contents (<1 wt%), and only a few pyroxene grains have TiO₂ contents up to 2 wt% (Table 2). Manganese contents show a positive correlation with iron contents (Fig. 8b) with Fe/Mn ratios of 41.5-83.7 (Table 2). The correlation is consistent with the lunar trend (Fig. 8b).

Olivine in Dhofar 1180 also has a large chemical variation (Table 3). Similar to pyroxene, olivine grains in most feldspathic lithic clasts (C-4, C-5, C-7, C-9, C-12, and C-13) and lithic clast C-8 are ferroan (Fa=31-41). Olivine grains in C-14 are the most magnesian with Fa components varying from 16.2 to 19.3. Oliving grains in C-6 and C-10 are also ferroan (Fa=44-45). Olivine grains in C-1, C-3, C-11, and C-15 are moderately to extremely Fe-rich. Olivine grains in C-1 show a large compositional variation among different grains (Fa=53.2-83). Olivine grains in C-3 and C-11 have a narrow chemical variation (Fa=68.7-69 and 87.5-87.8. respectively). Fayalite grains in C-15 have the lowest Mg# values (Fa=97.7). Olivine fragments in the matrix and glass clasts have a compositional range of Fa from 44 to 97.8. The Fe/Mn ratios of olivine vary from 70.5 to 131 (Table 3) and plot along the lunar trend (Fig. 8a).

Plagioclase grains in Dhofar 1180 are highly calcic with a small compositional range ($An_{90.3-98}$). Plagioclase grains in feldspathic lithic clasts and lithic clast C-8 have An components from 93.8 to 98. In some mafic lithic clasts (C-1, C-2, C-3, C-6, and C-10), plagioclase is relatively Na-rich with An value down to 90.3. Feldspars in C-15 have high components of Or and Ab ($Or_{61.5-65.2}Ab_{28.6-31.4}An_{6.2-7.2}$). Low total values (96.47–97.32 wt%) of these alkali feldspar grains

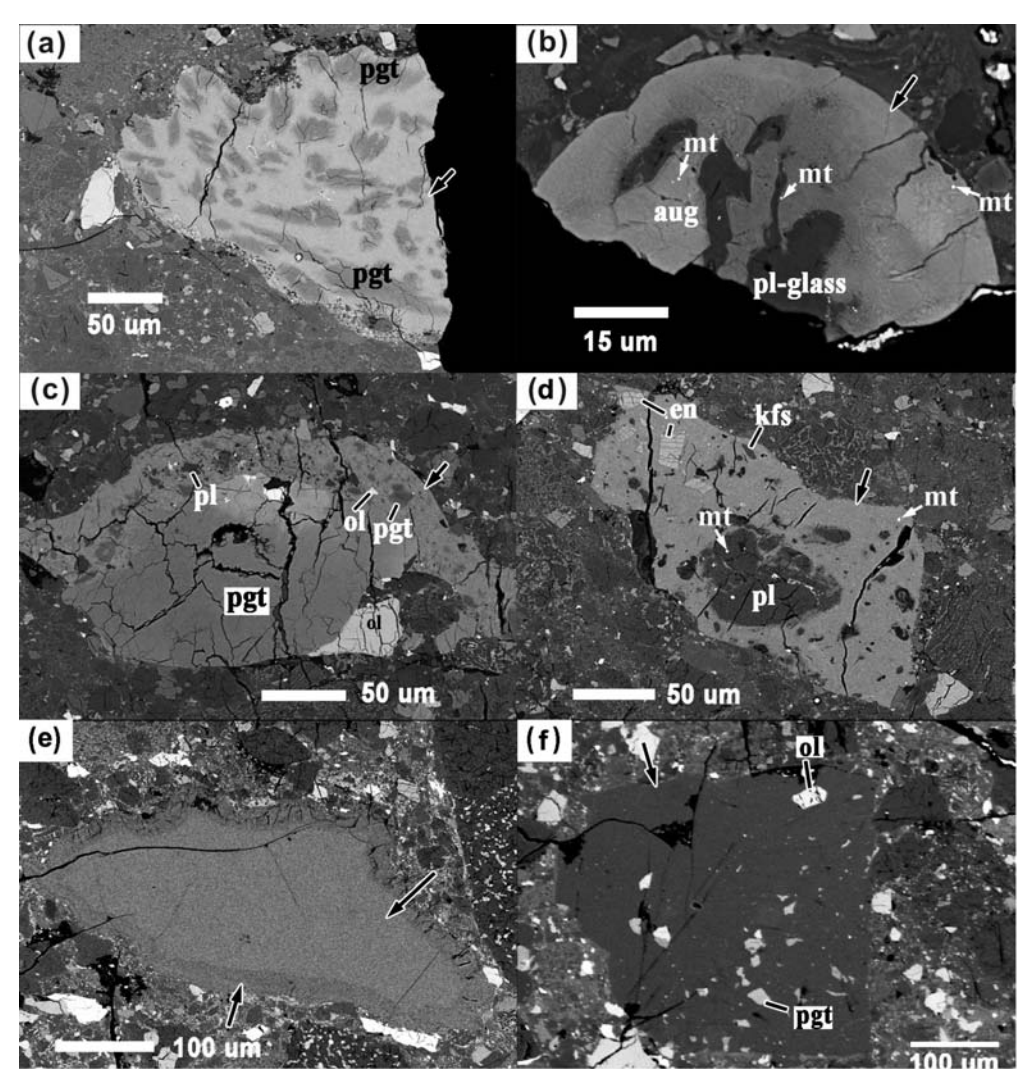


Fig. 4. BSE images of glasses in Dhofar 1180. a) A mafic glass including some anhedral-subhedral pigeonite grains. b) A mafic glass with a near-circular outline. This glass includes a relict augite grain and plagioclase glass. The glass portion shows devitrification. Some very fine-grained metal grains exist in this glass. c) A mafic glass that is attached to a pyroxene grain. d) A mafic glass containing some plagioclase grains, and fragments of exsolved enstatite and K-rich feldspar. Some very fine-grained metal grains exist in this glass. e) A feldspathic glass showing devitrification at the margin. Arrows indicate glass regions. pgt=pigeonite; aug=augite; ol=olivine; pl=plagioclase; kfs=K-rich feldspar; en=enstatite; mt=metal.

are probably due to evaporation loss of Na and K under high electron beam current or a small amount of BaO which is not analyzed. Plagioclase fragments have high An components (95.6–97.8) similar to those in feldspathic lithic clasts.

Most ilmenite grains in Dhofar 1180 have low MgO contents (Table 5). Ilmenite grains in C-4 and C-10 contain MgO up to 5.25 wt%. Ulvöspinel-chromite-hercynite/spinel solid solution has a large compositional variation (Usp_{0.5-97.4}Chr_{0.1-52.8}Hc/spl_{2.5-94.4}) among different lithic clasts and fragments. Oxide minerals are present as ulvöspinel and chromite in most lithic clasts, but as spinel in C-14 (Table 5).

Both apatite and merrillite occur in C-15. Apatite contains Cl (2.14–2.54 wt%) and F (1.59–1.89 wt%) (Table 6). Apatite has lower La_2O_3 (0.08–0.13 wt%), Ce_2O_3 (0.38–0.41 wt%), and Y_2O_3 (0.28–0.35 wt%) contents than merrillite (1.04–1.2 wt%,

2.54–3.01 wt%, 3.27–3.75 wt%, respectively). Apatite grains also have lower FeO (1.14–1.4 wt%), MgO (up to 0.11 wt%), and higher Al_2O_3 (0.24–0.85 wt%) contents than merrillite (4.76–6.71 wt%, 0.33–0.58 wt%, and 0.09–0.3 wt%, respectively).

Both kamacite and taenite occur in Dhofar 1180 (Table 7). Taenite contains higher Co content (1.53–2.32 wt%) than kamacite (0.54 wt%). The Ni/Co ratio varies from 12.8 to 24.5 and is similar to that of other lunar meteorites (e.g., Koeberl et al. 1996). Troilite contains very low Co (0.07–0.12 wt%) and Ni (<0.34 wt%).

Glass Compositions

Representative EMP analyses of glasses (Figs. 2c and

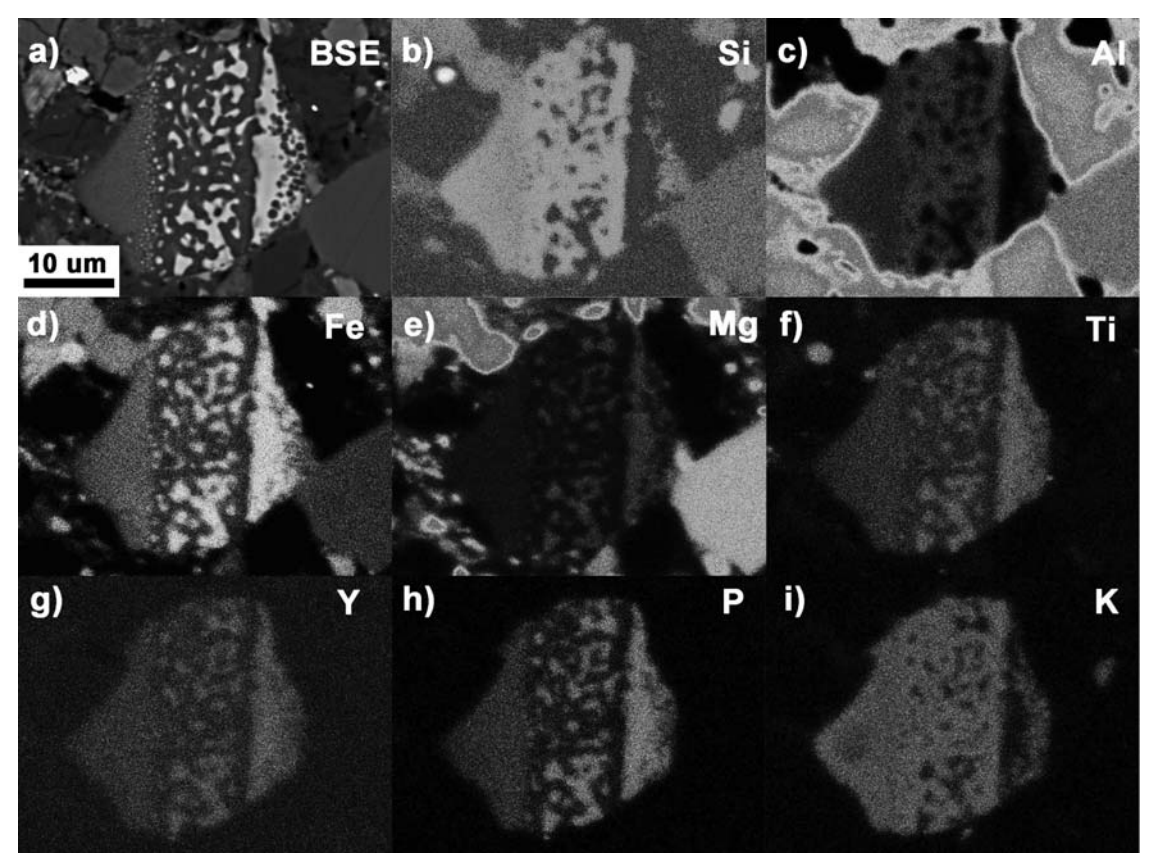


Fig. 5. BSE image (a) and X-ray mapping of Si (b), Al (c), Fe (d), Mg (e), Ti (f), Y (g), P (h), and K (i) of the P-rich glass in Dhofar 1180. The glass (on BSE image) consists of three portions with different textures: left portion (L), right portion (R) containing some sub-micron spherules, and middle portion (M) with a vermiform mixture of two immiscible glasses.

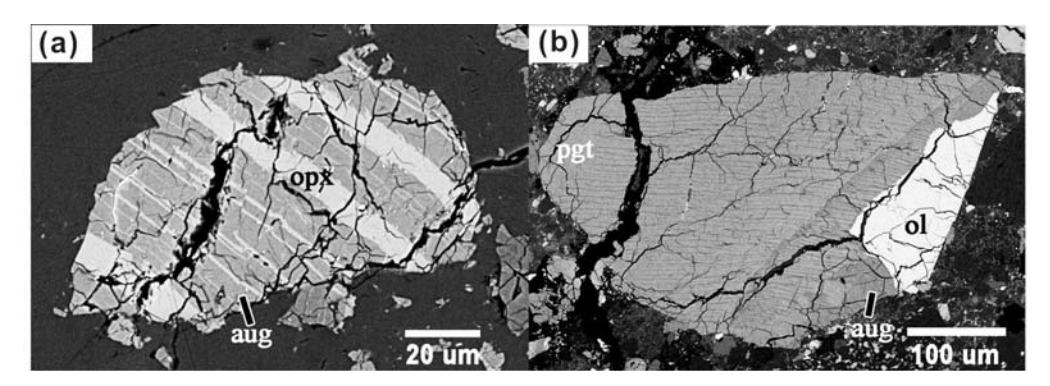


Fig. 6. BSE images of pyroxene fragments in Dhofar 1180. a) A pyroxene grain with coarse exsolution lamellae (up to 9 μ m). b) A pyroxene with fine exsolution lamellae (<2 μ m) coexists with olivine.

Table 1. Modal abundances (area%) of typical lithic clasts in Dhofar 1180.

	C-1	C-2	C-3	C-4	C-5	C-6	C-7	C-8	C-9	C-10	C-11	C-12	C-13	C-14	C-15
Feldspar Pyroxene Olivine	18.3 80.9 0.5	31.1 62.6	64.5 25.8 3.9	90.3 7.7 1.7	79 20.5 0.5	21.1 9 68.9	85.2 12.1 1.7	52 5.8 42.2	93.7 3.3 2.7	36.9 30.2 29	44.9 34.8	68.6 22.4 9.1	79.3 6.6 9.5	62.3 1.6 35	1.0 15.2 81.7
Oxide Silica Phosphate Troilite	0.3	6.3	5.8	0.3		1	1.0		0.3	3.9	20.3		4.6	1.1	0.85 0.5 0.5 0.25

Oxide including ilmenite and ulvöspinel-hercynite/spinel-chromite.

4–5) are given in Table 8. The Ca, Al-rich glass in C-2 has a similar composition to plagioclase but with a relatively high FeO content (2.65 wt%) (Table 8). The Si, K-rich glass in C-2 has 81.72 wt% SiO₂, 2.33 wt% K₂O, 3.18 wt% FeO, and 9.45 wt% Al₂O₃.

Mafic glasses with mineral inclusions have moderate to high FeO contents (14.78–38.26 wt%) and low MgO contents (2.16–8.1 wt%). The Mg# values vary from inclusion to inclusion (0.07–0.45). Al $_2$ O $_3$ content (2.29 to 15.29 wt%) varies among different glasses whereas the variation of CaO content among different glasses is relatively small (8.43–11.88 wt%). TiO $_2$ content of these glasses mainly varies from 4.39 wt% to 6.72 wt%; however, in one glass (Fig. 4b), the range of TiO $_2$ content is from 1.93 to 9.89 wt% (Table 8). Most glasses have low P_2 O $_5$ content (<0.32 wt%); however, P_2 O $_5$ content of the glass shown in Fig. 4d is up to ~1 wt%.

Mafic glasses without mineral inclusions have two compositional trends. They differ in major (Mg, Fe, Al, and Ca) as well as minor (Ti, Cr, K, and P) element concentrations. Group-1 is moderate Ti-rich (2.06–2.89 wt%) and contains high K_2O and P_2O_5 contents (0.25–0.51 wt% and 0.03– 0.54 wt%, respectively). MgO, FeO, Al₂O₃, and CaO contents are 8.05-9.78 wt%, 11.29-13.75 wt%, 15.07-16.98 wt%, and 9.80–10.63 wt%, respectively. The Cr₂O₃ content is low (0.2-0.26 wt%). The Mg# values of these glasses range from 0.53 to 0.61. Group-2 has very low contents of TiO₂ (0.25– 0.32 wt%), K_2O (0.01–0.06 wt%), and P_2O_5 (<0.03 wt%). Glasses in this group contain 10.94-11.34 wt% MgO, 10.08-10.59 wt% FeO, 17.12-17.37 wt% Al₂O₃, and 10.54-10.83 wt% CaO. Group-2 glasses have higher Mg# values (0.65-0.67) and Cr_2O_3 content (0.41-0.47 wt%) than Group-1 glasses.

Feldspathic glasses free of mineral inclusions have Al_2O_3 content ranging from 28.95 to 30.55 wt% (Table 8). MgO and FeO contents are relatively low (2.86–3 wt% and 4.50–4.77 wt%, respectively). These glasses contain 1.28–1.5 wt% TiO₂. The Mg# values are 0.52–0.54.

Feldspathic glasses with mineral inclusions have a composition similar to that of feldspar with high Al_2O_3 (35.79–36.04 wt%) and low MgO (0.06–1.33 wt%) and FeO (0.2–1.13 wt%) contents. TiO_2 contents (<0.08 wt%) of these glasses are lower than those without mineral inclusions.

In the P-rich glass (Fig. 5a), the right portion (R) is FeOrich (17.96 wt%) and contains relatively high contents of MgO (5.49%), CaO (9.14 wt%), TiO₂ (6.02 wt%), and P₂O₅ (6.25 wt%). Its Mg# value is 0.26. The dark glass in the middle portion (M_D in Table 8) is relatively rich in SiO₂ (60.24 wt%), Al₂O₃ (12.66 wt%), and K₂O (2.91 wt%). The left portion (L) has an intermediate chemical composition between R and M_D, similar to the average composition of the middle portion (M). The low total values may be due to a small amount of BaO, which was not included in the analyses. Distributions (Fig. 5) of element (Si, Al, Fe, Mg, Ti, P, and K) in different regions of the glass are consistent with the EMPA data (Table 8). Furthermore, the X-ray mapping

and EMPA data indicate that some trace elements (e.g., La, Th, Y, and Ce) are mainly concentrated in the right Fe-rich portion (Table 8).

Trace Element Concentrations

Concentrations of iron and trace elements of one 91.19 mg rock chip of Dhofar 1180 are given in Table 9. The bulk compositions of Calcalong Creek (Hill and Boynton 2003), Sayh al Uhaymir (SaU) 300 (Hsu et al. 2008), as well as data for Yamato 793274 (Koeberl et al. 1991), Elephant Moraine (EET) 96008 (Anand et al. 2003), Queen Alexandra Range (QUE) 94281 (Jolliff et al. 1998), are also listed for comparison. In our Dhofar 1180 sample, only 4.91 wt% Fe (=6.31 wt% FeO) was detected, lower than that (9.3 wt% FeO) reported by Bunch et al. (2006), which is probably due to sampling bias.

Concentration of lithophile element Sc is 15.53 ppm and the Fe/Sc ratio is 3167, lower than the average highland Fe/Sc value (4000, Palme et al. 1991). Concentrations of siderophile elements Co, Ni, and Ir in Dhofar 1180 are 15.68 ppm, 112 ppm, and 3.6 ppb, respectively, lower than those of SaU 300 (Table 9) and lunar regolith (e.g., Apollo 16 regolith). Concentrations of Sr (1973 ppm) and Ba (594 ppm) are high in Dhofar 1180, indicating terrestrial weathering in hot desert.

The CI-normalized (Anders and Grevesse 1989) REE pattern of Dhofar 1180 is shown in Fig. 9, along with those of other lunar meteorites (Calcalong Creek, Y-983885, Y-793274, EET 96008, QUE 94281, and SaU 300). Dhofar 1180 has a slightly LREE-rich (La 18 × CI, Sm 14 × CI) pattern with a small positive Eu anomaly (Eu 15 × CI). Our Dhofar 1180 sample contains 0.696 ppm Th, lower than that (0.9 ppm) reported by Bunch et al. (2006) and Korotev et al. (2008).

DISCUSSION

Mineralogy and petrology show that Dhofar 1180 is a polymict lunar regolith breccia. Fe-Mn ratios of olivine and pyroxene in Dhofar 1180 generally plot along the lunar trends, suggesting a lunar origin of Dhofar 1180. However, as observed in other lunar meteorites (e.g., Dhofar 025/081, Cahill et al. 2004; SaU 300, Hsu et al. 2008), Fe-Mn data of pyroxene from Dhofar 1180 (Fig. 8) plot well along the lunar trend at Fe > 1 apfu (atoms per formula unit), but data plot between the lunar and the Earth trends at Fe < 1 apfu. Cahill et al. (2004) explained that such a variation is due to the difference in lithologies analyzed in their study compared to that by Papike (1998). It is also possible that the full suite of lunar rocks is more variable than the subset plotted by Papike (1998). In addition, the high anorthite content of plagioclase is also consistent with a lunar origin. The fact that numerous glassy clasts exist in Dhofar 1180 suggests that Dhofar 1180 is a regolith breccia rather than a crystalline melt breccia as suggested by Bunch et al. (2006). In particular, some mafic glasses with mineral crystals (e.g., Figs. 4c-d) from Dhofar

Table 2. Representative electron microprobe analyses (wt%) of pyroxene in Dhofar 1180.

		C-1			C-2			C-3	C	-4		C-5	С	-6	С	-7	C-8	C-	-9
SiO_2	44.9	46.4	49.9	49.3	44.5	49.1	50.9	50.1	51.5	51.2	51.4	51.5	52.1	50.8	52.2	54.0	54.2	49.5	52.9
TiO_2	1.12	0.53	1.16	0.91	0.86	0.71	0.52	0.83	0.69	0.74	0.81	0.77	0.54	0.99	0.61	0.46	0.75	1.07	0.64
Al_2O_3	0.94	0.39	2.00	2.57	1.45	0.98	0.50	0.79	1.14	1.41	1.01	0.96	0.66	1.92	0.75	0.58	0.67	4.58	0.59
Cr_2O_3	0.03	bd	1.00	0.86	0.03	0.28	0.20	0.16	0.35	0.45	0.40	0.35	0.31	0.68	0.24	0.20	0.30	0.65	0.30
MgO	0.61	0.15	12.8	15.9	0.13	12.3	10.2	10.8	20.7	20.0	20.8	21.5	19.9	14.5	21.4	21.8	23.3	16.6	19.8
FeO	42.0	45.8	13.4	17.4	42.1	31.0	20.8	28.3	19.0	17.6	19.6	20.5	23.3	11.4	18.5	20.1	14.5	14.2	20.0
MnO	0.59	0.54	0.26	0.35	0.53	0.54	0.35	0.41	0.33	0.33	0.38	0.37	0.47	0.27	0.33	0.34	0.24	0.29	0.31
CaO	8.46	5.60	17.3	11.4	9.06	5.71	15.8	8.60	5.31	6.75	5.47	4.25	2.67	18.7	5.32	2.44	5.29	13.0	4.41
Na_2O	0.02	0.02	0.08	0.02	0.02	bd	0.09	0.34	bd	0.02	0.02	bd	bd	0.10	0.02	0.02	0.04	0.07	0.03
K_2O	0.02	0.03	bd	bd	bd	bd	bd	bd	bd	bd	bd	0.02	bd	bd	bd	0.02	bd	bd	0.02
P_2O_5	bd	_	_	bd	0.07	bd	_	_	bd	bd	bd	bd	0.02	0.03	0.04	_	bd	0.04	bd
Total	98.69	99.46	97.9	98.71	98.75	100.6	99.36	100.3	99.02	98.5	99.89	100.2	99.97	99.33	99.41	99.96	99.29	100	99
En	2.0	0.5	39.3	47.3	0.4	36.6	30.8	33.1	59.1	57.8	58.4	59.8	57.2	42.4	60.3	62.8	66.3	49.2	58.1
Fs	77.8	86.0	22.8	28.6	78.0	51.2	34.9	48.1	30.1	28.3	30.6	31.7	37.3	18.5	29.0	32.2	23.0	23.3	32.6
Wo	20.2	13.5	37.9	24.1	21.6	12.2	34.3	18.8	10.8	14.0	11.0	8.5	5.5	39.1	10.7	5.0	10.8	27.5	9.2
Mg#	0.03	0.01	0.63	0.62	0.01	0.42	0.47	0.41	0.66	0.67	0.66	0.65	0.61	0.70	0.68	0.66	0.74	0.68	0.64
Fe/Mn	70.2	83.7	50.7	48.9	78.3	56.5	58.5	68.0	56.7	52.5	50.8	54.6	48.8	41.5	55.4	58.4	59.7	48.1	63.7

Table 2. Continued. Representative electron microprobe analyses (wt%) of pyroxene in Dhofar 1180.

	C-	10	C	-11	C	-12	C-	13	C	-14	C	-15			Frag	ment		
SiO_2	52.0	50.2	47.7	48.6	50.2	49.9	52.1	52.6	55.3	54.4	44.8	44.0	45.3	50.3	50.4	45.7	55.3	51.1
TiO_2	0.87	0.96	0.98	0.91	0.86	0.87	0.73	0.68	0.55	0.74	1.66	1.53	0.60	0.14	0.87	1.13	0.20	0.58
Al_2O_3	1.16	4.62	1.17	1.24	1.82	2.11	1.17	0.93	1.10	2.18	3.73	2.47	0.57	0.26	1.73	1.19	1.11	2.90
Cr_2O_3	0.33	0.35	0.16	0.13	_	_	0.33	0.30	0.19	0.25	0.04	0.05	Bd	0.11	0.31	_	0.39	1.06
MgO	19.1	17.0	5.30	5.33	20.9	16.7	21.4	21.7	29.2	28.7	0.97	1.06	0.25	12.6	9.90	4.79	28.2	15.8
FeO	22.3	19.8	27.2	28.4	19.7	13.8	21.1	19.5	8.86	9.01	28.4	30.5	44.2	34.4	15.1	34.4	12.9	11.1
MnO	0.38	0.36	0.48	0.48	0.40	0.24	0.35	0.36	0.23	0.17	0.37	0.37	0.76	0.63	0.29	0.52	0.27	0.25
CaO	4.11	6.45	16.5	15.5	5.25	15.1	2.85	4.30	3.74	4.16	19.5	20.1	7.24	0.87	20.9	10.9	1.43	17.0
Na ₂ O	0.03	0.04	0.09	0.06	0.02	0.02	0.03	0.02	0.05	0.02	0.10	0.24	bd	bd	0.06	bd	0.04	0.05
K_2O	bd	bd	bd	0.02	bd	0.02	0.07	bd	bd	0.02	bd	0.02	bd	bd	bd	bd	0.02	bd
P_2O_5	0.03	bd	0.05	0.02	0.02	bd	0.03	0.02	bd	bd	0.07	bd	bd	bd	bd	bd	bd	0.02
Total	100.3	99.78	99.63	100.7	99.17	98.76	100.2	100.4	99.22	99.65	99.64	100.3	98.92	99.31	99.56	98.63	99.86	99.86
En	55.5	52.2	16.4	16.6	58.7	47.4	60.8	61.0	79.3	78.2	3.2	3.3	0.8	39.0	29.8	15.1	77.4	46.3
Fs	36.0	33.7	46.9	49.0	30.7	21.8	33.4	30.4	13.4	13.7	51.4	52.3	81.9	59.1	25.2	60.3	19.7	18.0
Wo	8.5	14.1	36.7	34.4	10.6	30.7	5.8	8.6	7.3	8.1	45.4	44.4	17.3	1.9	45.0	24.6	2.8	35.7
Mg#	0.61	0.61	0.26	0.25	0.66	0.68	0.65	0.67	0.86	0.85	0.06	0.06	0.01	0.40	0.54	0.20	0.80	0.72
Fe/Mn	57.8	54.3	55.9	58.3	48.5	56.7	59.4	53.4	38.0	52.3	75.8	81.2	57.3	53.9	51.2	65.3	47.2	43.6

Bd: below detection limit; -: not analyzed. En: enstatite; Fs: ferrosilite; Wo: wollastonite.

Table 3. Representative electron microprobe analyses (wt%) of olivine in Dhofar 1180.

	C	:-1	(C-3	C	:-4	(C-5	C	C-6		C-7	C	:-8	(C-9
SiO_2	30.7	34.0	33.2	33.1	35.6	35.4	35.6	35.4	35.2	36.2	35.1	37.1	38.4	37.6	34.9	36.8
TiO_2	0.18	0.08	0.37	0.13	0.08	0.09	0.04	0.04	0.07	0.05	bd	bd	0.04	0.08	0.03	0.05
Al_2O_3	bd	0.02	bd	0.06	0.24	0.03	0.09	0.02	bd	0.02	0.07	0.02	0.23	0.07	0.11	0.02
Cr_2O_3	bd	0.03	bd	bd	0.06	0.07	0.07	0.04	0.06	0.08	bd	bd	0.08	0.05	0.07	0.05
MgO	6.96	21.5	13.0	13.1	30.1	29.6	32.7	30.1	25.5	26.5	30.6	29.5	34.0	33.7	29.3	28.2
FeO	61.1	44.0	52.0	51.8	33.9	33.8	30.0	33.4	39.7	36.9	33.1	32.4	26.9	27.2	34.7	34.9
MnO	0.70	0.48	0.52	0.62	0.34	0.32	0.31	0.33	0.47	0.38	0.34	0.31	0.28	0.25	0.37	0.33
CaO	0.40	0.26	0.29	0.21	0.33	0.22	0.22	0.17	0.19	0.25	0.12	0.15	0.11	0.07	0.28	0.36
Na ₂ O	bd	bd	0.06	bd	0.03	bd	0.02	bd	bd	bd	bd	0.02	bd	bd	bd	bd
K_2O	bd	0.02	bd	0.03	0.02	bd	bd									
P_2O_5	0.05	bd	_	_	bd	bd	0.03	0.06	0.03	_	bd	_	_	_	bd	_
Total	100.1	100.4	99.44	99.02	100.7	99.53	99.08	99.56	101.2	100.4	99.35	99.5	100.1	99.04	99.76	100.7
Fa	83	53	69	69	38	39	34	38	46	46	38	38	31	31	40	41
Mg#	0.17	0.47	0.31	0.31	0.62	0.61	0.66	0.62	0.54	0.56	0.62	0.62	0.69	0.69	0.60	0.59
Fe/Mn	86.0	90.4	98.7	82.3	98.4	104.1	95.6	99.7	83.3	95.8	95.9	102.9	94.7	107.3	92.5	104.3

Table 3. Continued. Representative electron microprobe analyses (wt%) of olivine in Dhofar 1180.

<u>, </u>	C	:-10	C	:-11	C	-12	C-	-13	C-	-14	C	:-15		Frag	gment	
SiO_2	34.9	34.5	30.4	30.8	35.5	35.8	35.7	35.9	39.4	39.2	30.1	30.0	33.5	32.3	29.9	29.2
TiO_2	0.23	0.56	0.06	0.07	0.11	0.06	0.04	bd	0.11	0.16	0.12	0.11	0.15	0.04	0.26	0.20
Al_2O_3	0.02	0.20	bd	0.10	0.38	0.23	bd	0.03	0.10	0.50	bd	0.02	0.03	bd	bd	bd
Cr_2O_3	0.06	0.08	bd	bd	_	_	0.03	0.02	0.06	0.04	0.03	bd	bd	0.12	0.05	0.02
MgO	25.9	25.6	4.84	4.87	31.9	32.6	31.3	31.1	44.3	40.0	0.79	0.89	26.1	15.9	6.24	1.15
FeO	37.8	37.7	62.5	61.6	31.4	31.0	32.2	31.5	15.6	17.2	66.5	67.3	40.1	50.5	61.3	67.5
MnO	0.41	0.39	0.84	0.78	0.29	0.32	0.28	0.34	0.15	0.24	0.84	0.90	0.47	0.56	0.76	0.85
CaO	0.18	0.27	0.30	0.97	0.26	0.33	0.14	0.19	0.11	0.24	0.62	0.64	0.32	0.49	0.55	0.43
Na ₂ O	bd	bd	0.02	0.03	bd	bd	0.02	bd	bd	0.05	0.04	bd	0.02	bd	0.02	bd
K_2O	bd	bd	bd	bd	bd	bd	bd	bd	bd	0.02	bd	bd	bd	bd	bd	bd
P_2O_5	bd	bd	0.14	bd	0.04	0.02	bd	0.02	bd	bd	0.02	0.06	_	bd	0.04	bd
Total	99.5	99.3	99.1	99.22	99.88	100.4	99.71	99.1	99.83	97.65	99.06	99.92	100.7	99.91	99.12	99.35
Fa	45	45	88	88	35	35	36	36	16	19	98	98	46	64	85	97
Mg#	0.55	0.55	0.12	0.12	0.65	0.65	0.64	0.64	0.84	0.81	0.02	0.02	0.54	0.36	0.15	0.03
Fe/Mn	91.0	95.2	73.4	77.9	106.9	95.6	113.2	91.3	102.5	70.5	78.1	73.7	84.2	88.8	79.5	78.4

Bd: below detection limit; -: not analyzed. Fa: fayalite.

TC 1.1 4 D	1		1 ((07)		TZ ' 1 C 1 1	' D1 C 1100
Table 4 Re	enresentative electro	n microprobe ai	nalyses (wt%)	of anorthite and	K-rich feldspar	in Dhotar 1180

	C-1		C-2	(C-3		C-4		C-5		C-6		C-7	C-8
SiO_2	44.4	46.5	45.4	41.8	41.8	43.9	43.6	43.2	41.8	44.1	45.0	43.0	43.7	41.7
TiO_2	0.06	0.04	0.05	bd	bd	bd	0.06	bd	bd	0.09	0.56	bd	0.03	bd
Al_2O_3	35.2	32.1	32.8	38.7	38.6	35.1	34.9	34.9	38.7	32.1	31.2	35.0	35.5	38.2
Cr_2O_3	0.02	bd	bd	0.03	0.02	bd	bd	bd	bd	0.10	0.05	bd	bd	0.02
MgO	0.31	0.09	0.15	bd	bd	0.07	0.09	0.09	0.12	0.37	0.73	0.03	0.04	0.08
FeO	1.35	1.15	0.72	0.28	0.45	0.31	0.35	0.34	0.29	1.21	3.25	0.15	0.15	0.16
MnO	0.02	0.02	0.02	0.03	bd	bd	bd	0.04	0.02	0.05	0.06	bd	bd	bd
CaO	17.7	17.5	18.1	19.3	19.2	19.5	19.7	19.4	19.3	18.6	17.0	19.5	19.6	18.9
Na ₂ O	0.93	1.00	0.83	0.54	0.54	0.35	0.31	0.42	0.43	0.47	0.70	0.39	0.36	0.45
K_2O	0.05	0.07	0.03	0.05	0.08	0.03	bd	0.03	0.03	0.08	0.06	0.03	0.04	0.02
P_2O_5	_	0.04	bd	_	_	bd	0.05	0.03	_	bd	_	0.02	bd	_
Total	100.0	98.51	98.1	100.7	100.7	99.26	99.06	98.45	100.7	97.17	98.61	98.12	99.42	99.53
An	91.1	90.3	92.2	94.9	94.7	96.7	97.2	96.1	96.0	95.2	92.7	96.3	96.6	95.8
Or	0.3	0.4	0.2	0.3	0.5	0.2	0	0.2	0.2	0.5	0.4	0.2	0.2	0.1

Table 4. Continued. Representative electron microprobe analyses (wt%) of anorthite and K-rich feldspar in Dhofar 1180.

	(C-9		:-10	C	:-12	C	-13	C	-14		C-15		Fragme	nt
SiO_2	43.0	42.1	44.6	43.1	42.8	43.3	43.8	43.3	44.3	43.6	64.2	62.5	41.9	41.9	44.7
TiO_2	bd	0.09	0.13	0.12	0.03	bd	0.05	bd	0.03	bd	0.43	0.39	bd	bd	bd
Al_2O_3	35.	37.8	33.3	35.2	34.7	34.4	36.2	36.4	36.0	36.5	20.4	20.1	38.2	37.2	35.2
Cr_2O_3	bd	bd	bd	0.02	_	_	0.09	bd	bd	bd	bd	_	bd	bd	0.04
MgO	0.14	0.16	0.32	0.41	0.08	0.17	0.11	0.09	0.16	0.09	bd	0.10	0.16	0.15	0.08
FeO	0.29	0.25	0.71	0.77	0.49	0.49	0.35	0.24	0.37	0.22	0.82	0.68	0.33	0.35	0.28
MnO	bd	bd	0.02	bd	0.06	bd	bd	bd	bd	bd	0.03	bd	bd	bd	bd
CaO	19.2	18.1	19.0	19.8	20.4	19.7	19.4	19.6	19.0	20.0	0.48	0.63	19.1	19.0	19.4
Na ₂ O	0.42	0.43	0.52	0.15	0.30	0.41	0.42	0.34	0.53	0.22	2.45	3.04	0.45	0.47	0.23
K_2O	bd	0.10	0.02	0.02	0.02	0.05	0.04	0.03	0.02	bd	8.48	9.04	0.03	0.03	bd
P_2O_5	bd	bd	0.02	0.04	bd	0.03	bd	bd	bd	bd	0.03	0.03	_	_	_
Total	98.05	99.03	98.64	99.63	98.88	98.55	100.5	100	100.4	100.6	97.32	96.51	100.2	99.1	99.93
An	96.2	95.3	95.2	98.5	97.3	96.1	96.0	96.8	95.1	98.0	3.2	3.7	95.8	95.6	97.9
Or	0	0.6	0.1	0.1	0.1	0.3	0.2	0.2	0.1	0	67.3	63.8	0.2	0.2	0

Bd: below detection limit; -: not analyzed. An: anorthite; Or: orthoclase.

Table 5. Representative electron microprobe analyses (wt%) of oxide minerals in Dhofar 1180.

		C-1		2-2		C-3	C-4	(C-6		:-7	(C-9
SiO_2	0.03	0.41	0.09	0.05	0.04	bd	0.79	0.13	0.05	0.12	0.66	0.04	0.20
TiO_2	53.3	35.2	33.6	52.7	25.3	51.5	53.7	9.67	16.2	17.7	25.8	21.7	15.2
Al_2O_3	0.06	1.41	1.82	0.06	2.15	bd	0.46	9.81	6.73	5.55	4.99	5.30	7.66
Cr_2O_3	0.18	2.96	0.63	bd	12.8	0.10	0.36	36.4	29.0	27.4	25.1	21.1	28.8
MgO	0.24	0.32	0.14	0.02	0.64	0.99	5.25	2.44	2.92	3.94	3.74	4.41	3.77
FeO	46.0	58.8	63.4	46.9	58.2	46.5	39.1	39.0	43.6	44.6	38.8	47.1	42.9
MnO	0.45	0.36	0.43	0.40	0.46	0.37	0.41	0.43	0.41	0.39	0.36	0.38	0.37
CaO	0.21	0.29	0.11	0.19	0.06	bd	0.68	0.20	0.22	0.48	0.43	0.38	0.60
Total	100.5	99.75	100.2	100.3	99.65	99.46	100.8	98.08	99.13	100.2	99.88	100.4	99.5
Нс		2.9	4.0		5.0			21.1	14.4	11.9	9.1	11.2	16.5
Chr		4.1	0.9		19.9			52.4	41.5	39.5	30.8	30.0	41.7
Usp		93.0	95.0		75.1			26.5	44.1	48.6	60.1	58.7	41.8

Table 5. Continued. Representative electron microprobe analyses (wt%) of oxide minerals in Dhofar 1180.

		-10		C-13		C-14	C-15			Fragmen	t	
SiO_2	5.30	3.42	0.11	0.12	0.07	0.49	0.37	2.56	0.12	0.04	bd	0.10
TiO_2	48.9	49.7	13.0	13.0	0.26	0.24	50.5	30.3	33.3	19.1	54.0	51.5
Al_2O_3	1.57	0.94	10.0	8.87	59.2	63.6	0.21	4.08	1.09	6.51	0.02	0.05
Cr_2O_3	0.85	0.93	33.1	34.9	9.97	5.13	0.07	1.10	0.06	25.0	0.20	bd
MgO	4.57	4.20	3.31	4.07	18.2	19.3	0.08	0.68	0.09	4.03	0.23	0.02
FeO	38.8	40.6	39.5	38.6	13.4	11.9	47.6	55.2	64.7	44.0	45.8	46.5
MnO	0.35	0.38	0.36	0.38	0.11	0.11	0.40	0.06	0.39	0.38	0.44	0.42
CaO	1.24	0.63	0.17	0.25	0.07	0.21	0.42	0.73	0.24	0.11	0.04	0.48
Total	101.6	100.8	99.55	100.2	101.3	101	99.65	94.71	99.99	99.17	100.7	99.07
Hc			20.5	18.1	89.4^{*}	94.4*		9.4	2.5	13.6		
Chr			45.5	47.9	10.1	5.1		1.7	0.1	35.2		
Usp			34.0	33.9	0.5	0.5		88.9	97.4	51.1		

Bd: below detection limit; -: not analyzed. *: spinel. Hc: hercynite; Chr: chromite; Usp: ulvöspinel.

Table 6. Representative electron microprobe analyses (wt%) of phosphates in C-15 from Dhofar 1180.

or phosp	mates m	C 15 110	iii Diioia	1 1	100.		
		Apatite	:			Merrillit	e
SiO_2	3.56	3.78	2.91		2.29	2.04	4.64
TiO_2	0.06	0.02	0.09		0.12	0.04	0.08
Al_2O_3	0.85	0.62	0.24		0.30	0.09	0.16
MgO	0.11	bd	bd		0.36	0.33	0.58
FeO	1.14	1.23	1.40		4.76	5.49	6.71
CaO	51.4	50.7	51.6		37.5	38.5	37.3
Na_2O	0.14	0.07	0.08		0.59	0.07	0.07
K_2O	0.07	0.10	0.02		0.10	0.04	0.04
P_2O_5	38.0	38.8	38.4		44.6	44.4	42.7
La_2O_3	0.08	0.13	0.10		1.20	1.07	1.04
Ce_2O_3	0.38	0.40	0.41		3.01	2.76	2.54
Y_2O_3	0.28	0.30	0.35		3.27	3.75	3.39
Cl	2.14	2.53	2.54		0.04	bd	bd
F	1.89	1.89	1.59		bd	bd	bd
Total	98.82	99.23	98.52		98.13	98.55	99.27

bd: below detection limit.

1180 are similar in petrographic texture to agglutinates of lunar regolith (Papike et al. 1998).

Affinity of Non-Mare Lithic Clasts to Ferroan Anorthositic Suite and Magnesian Suite Rocks

Most lithic clasts (e.g., C-4, C-5, C-7, C-9, C-12, C-13, and C-14) in Dhofar 1180 are feldspathic. On the Mg# versus AN diagram (Fig. 10), they fall in the region of ferroananorthositic suite rocks. This suggests that most feldspathic lithic clasts in Dhofar 1180 have a strong affinity to ferroananorthositic suite rocks of highlands origin. Modal abundance and mineral assemblage in these clasts also support this conclusion. They contain a high abundance of plagioclase $(>\sim70\%)$ except C-14 $(\sim60\%)$. C-14 plots in the magnesian suite region defined by Apollo mafic non-mare rocks (Fig. 10). Modal abundance of this clast (Table 1) suggests that it is a spinel anorthositic troctolite. This lithic clast does contain incompatible-trace-element-rich accessory minerals (e.g., phosphate), probably indicating that it is not related to KREEP rocks. In contrast, magnesian suite rocks (including troctolites and spinel troctolites) in Apollo samples commonly contain some incompatible-trace-element-rich phases and are genetically related to KREEP rocks (Papike et al. 1998; Lucey et al. 2006). Furthermore, olivine in spinel troctolites (Fo₉₀₋₉₃) from Apollo samples (Papike et al. 1998) commonly has a higher Mg# than that in C-14 (Fo₈₁₋₈₄). These differences indicate that spinel anorthositic troctolite in Dhofar 1180 probably represent a magnesian suite rock that is not genetically related to Apollo magnesian suite rocks. The compositional range of C-8 also plots within the region of ferroan-anorthositic suite rocks (Fig. 10), implying a possible affinity to ferroan anorthositic suite rocks.

On the diagram of Ti# (Ti/[Ti+Cr] in mole) versus Fe# (Fe/[Fe+Mg] in mole), pyroxene grains in these highlands

lithic clasts are Mg-rich (Mg# >60) and the variation of Fe# is very small within individual lithic clasts (see Fig. 11). Ti# shows a relatively large variation. A similar composition trend has been described in other lunar meteorites and Apollo samples (Arai et al. 1996). Arai et al. (1996) observed similar features in Yamato 793274 and suggested a highlands origin of these features. They interpreted that this trend could be caused by various diffusion rates of different elements in pyroxene. Diffusion rates of Ti and Cr are slower in pyroxene than those of Fe and Mg. When original pyroxenes zoned in terms of Ti# and Fe# underwent subsequent annealing processes, Fe# is more easily homogenized whereas Ti# is affected to a lesser extent (Arai et al. 1996). Although some slowly cooled mare gabbros (e.g., cumulate gabbro portion in NWA 773, Fagan et al. 2003) also show a similar trend, they usually have distinct mineral assemblages. Combining the petrography and mineralogy, the Ti#-Fe# variations indicate that most feldspathic lithic clasts in Dhofar 1180 could be of highlands origin.

Fe-Enrichment of Mafic Lithic Clasts and Affinity to Low-Ti Basalts

Although lithic clasts C-1, C-2, C-3, C-6, C-10, C-11, and C-15 show different petrographic textures and mineral assemblages from each other, mafic minerals in most of these clasts have much lower Mg# values than those of ferroan anorthositic suite rocks. They represent fragments of mare lithologies. However, various petrographic and mineralogical features suggest that they have different formation histories.

Although C-1 and C-2 have various rock textures, pyroxene grains in both clasts are zoned and they have a similar compositional range (e.g., Mg#=0.63-0.01 for pyroxene), possibly indicating a similar degree of Feenrichment. In these two clasts, chemical zoning of some pyroxene grains records a rapid fractionation crystallization of erupted basaltic melt. Moderate Mg# values (0.51-0.62) of pyroxene core probably imply a moderate Fe-enrichment of primary basaltic melt, and the appearance of pyroxferroite as pyroxene rims represents an extreme Fe-enrichment of latestage basaltic melt. Pyroxferroite has been interpreted as a metastable Fe-rich pyroxenoid (Lindsley et al. 1972), so its occurrence also indicates a non-equilibrium crystallization of basaltic melt. In addition, the existence of Si, K-rich glass also supports the extreme evolution of the basalt melt. Lithic clast C-3 is moderately Fe-rich compared to other mare lithic clasts. It might represent a hypabyssal igneous body, because fine-scaled exsolution lamellae of pyroxene reflect a relatively slow cooling rate, although most mare basalt samples do not exhibit such exsolution lamellae (Arai and Warren 1999). C-6 has a high modal abundance of mafic minerals and shows a porphyritic texture, which suggests that this clast is a basaltic clast. Augite exsolution in pigeonite and the fine-grained texture of the groundmass were probably

Table 7. Representative electron microprobe analyses (wt%) of FeNi metal and troilite in Dhofar 1180.

	Tae	Tae	Kam				Γroilite		
Fe	60.3	66.5	91.5	62.7	62.0	62.2	62.4	62.3	63.2
Ni	37.4	32.2	6.90	bd	0.13	0.10	0.34	bd	bd
Co	1.53	2.32	0.54	0.08	0.10	0.12	0.17	0.07	0.12
S	1.18	0.02	bd	36.8	37.4	36.8	36.7	36.8	36.6
Total	100.4	101	98.94	99.58	99.63	99.22	99.63	99.09	99.9
Ni/Co	24.5	13.9	12.8						

Kam: kamacite; Tae: taenite. bd: below detection limit.

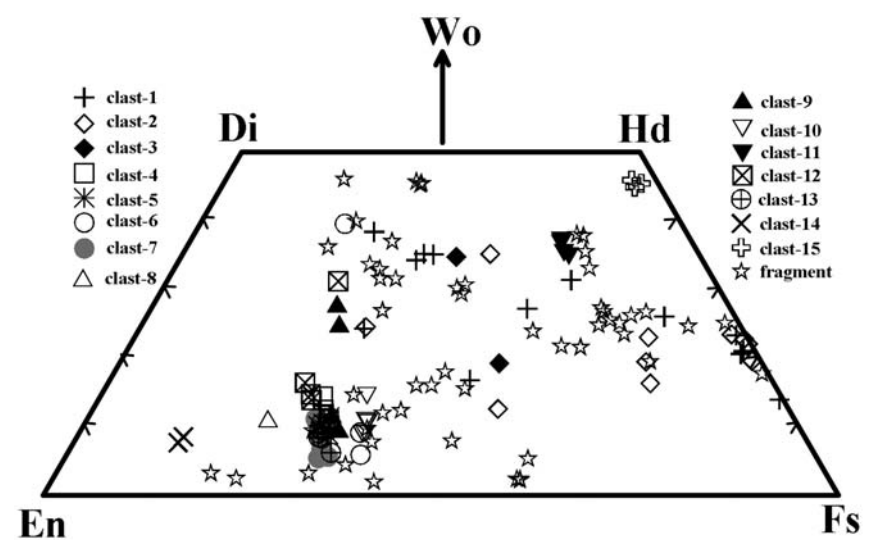


Fig. 7. Pyroxene compositions in Dhofar 1180 plotted on a pyroxene quadrilateral.

formed due to different processes. The former is probably related to slow cooling of the basalt, whereas the fine-grained texture of the groundmass is related to re-melting (probably shock melting) and a subsequent rapid cooling process. Although exsolution lamellae of a few microns in pyroxene are not common in Apollo basalts, similar features were also observed in some lunar meteorites (Arai and Warren 1999). C-10 also has a high modal abundance of mafic minerals. Mafic minerals in both C-6 and C-10 have relatively high Mg#, probably representing Mg-rich basalts.

The mineral assemblage of favalite, ferroaugite, and silica has been observed in other lunar breccias (e.g., QUE 94281, Jolliff et al. 1998; EET 96008, Anand et al. 2003; breccia portion of NWA 773, Fagan et al. 2003; Miller Range [MIL] 05035, Liu et al. 2009). This mineral assemblage indicates an extreme differentiation and Fe-enrichment with very low Mg# values (0.12 for fayalite and 0.25-0.26 for ferroaugite). Heating experiments by Lindsley et al. (1972) show that mineral assemblage of fayalite, Ca,Fe-rich pyroxene, and silica could have formed by decomposition of pre-existing pyroxferroite. This interpretation has been used to explain the origin of similar mineral assemblage in other lunar breccias (e.g., EET 96008, Anand et al. 2003). The mineral assemblage in Dhofar 1180 probably has a similar origin and reflects an unusual slow cooling rate. The texture of triple junction is also consistent with this explanation.

Lithic clast C-15 (Fig. 3) is generally similar in petrology and mineralogy to the fayalite gabbro in NWA 773 (Fagan et al. 2003). The extremely low Mg# values of olivine and pyroxene indicate that these clasts represent late-stage differentiates. The occurrence of K-rich feldspar, silica, apatite, REE-rich merrillite, troilite, and baddeleyite also supports this conclusion. These interstitial phases probably crystallized from residual alkali- and silica-rich liquids after crystallization of extremely Fe-rich minerals. The consolidation of C-15 is probably related to immiscibility of Fe-rich and Si-, K-rich liquids. Similar explanations have been proposed by previous investigations (e.g., Roedder and Weiblen 1978; Fagan et al. 2003).

Previous investigations (Arai et al. 1996; Joy et al. 2006) have proposed that pyroxenes from mare basalts commonly show a strong correlation between Fe# and Ti#. The correlation between Fe# and Ti# depends on chemical compositions of crystallizing basaltic magmas (Anand et al. 2003). Different bulk TiO₂ contents of basalts produce various trends. Nielsen and Drake (1978) and Treiman and Drake (1983) suggested that at any given Fe#, Ti# of pyroxene in very low-Ti basalts (TiO₂<1.5 wt%) tends to be systematically lower than that in Apollo-15 low-Ti basalts (1.5–6 wt%). In Dhofar 1180, the correlation between Fe# and Ti# of pyroxenes from mare lithic clasts are well consistent with the Apollo-15 low-Ti basalt trend (Fig. 11). Arai et al.

Table 8. Representative electron microprobe analyses (wt%) of glasses in Dhofar 1180.

	C-2							Mafic glasses without inclusions (group-1)		Mafic glasses without inclusions (group-2)		Feldspathic glasses without inclusions		Feldspathic glasses with inclusions		KREEPy			
	Ca,Al- rich	Si,K- rich	Mafic glasses with inclusions		R	MD	M									L			
SiO ₂	48.0	81.7	42.2	34.1	45.2	43.7	45.7	50.0	50.0	49.0	48.3	45.1	42.2	42.0	44.9	35.1	60.2	52.2	54.0
TiO_2	0.28	0.51	3.03	9.89	4.73	5.93	6.72	0.25	0.27	2.89	2.06	1.40	1.50	0.08	bd	6.02	2.36	3.25	2.77
Al_2O_3	30.1	9.45	7.36	5.36	7.40	11.9	9.31	17.3	17.2	15.1	16.8	29.0	30.6	36.1	35.8	6.61	12.7	11.0	11.7
Cr_2O_3	bd	0.02	0.07	0.09	0.31	0.28	0.07	0.41	0.41	0.23	0.22	0.08	0.12	0.03	bd	0.12	0.02	0.04	0.07
MgO	0.03	bd	2.16	2.70	7.57	7.16	1.15	11.3	11.0	8.97	9.78	2.86	2.83	1.33	0.06	5.49	1.56	2.60	2.34
FeO	2.65	3.18	33.4	38.3	24.5	16.0	26.3	10.1	10.5	13.8	11.3	4.50	4.70	1.13	0.20	28.0	9.53	14.0	12.5
MnO	0.02	bd	0.44	0.42	0.26	0.22	0.15	0.15	0.2	0.17	0.16	0.04	0.11	0.04	bd	0.36	0.14	0.18	0.21
CaO	16.3	1.15	10.0	8.43	9.80	11.7	8.91	10.8	10.8	9.89	10.3	16.7	16.6	19.0	19.4	9.14	5.70	7.10	6.35
Na_2O	0.97	0.71	0.09	0.08	0.08	0.31	0.70	0.14	0.25	0.25	0.39	0.46	0.61	0.59	0.50	0.15	0.63	0.51	0.48
K_2O	0.39	2.33	0.22	0.21	0.36	0.27	1.20	0.02	0.06	0.29	0.25	0.18	0.29	0.02	bd	0.70	2.91	2.75	3.08
P_2O_5	0.04	0.11	0.14	0.18	0.05	1.04	-	0.03	bd	0.03	0.12	0.08	-	_	bd	6.25	1.61	2.82	2.90
La_2O_3																0.04	0.01	bd	0.01
ThO_2																0.06	bd	0.02	bd
YO_2																0.17	0.10	0.08	0.09
Ce_2O_3																0.19	0.12	0.13	0.13
Total	98.78	99.16	99.11	99.76	100.3	98.51	100.2	100.5	100.7	100.6	99.68	100.4	99.56	100.3	100.9	98.4	97.59	96.68	96.63
Mg#			0.10	0.11	0.36	0.45	0.07	0.67	0.65	0.54	0.61	0.53	0.52	0.68	0.35	0.26	0.23	0.25	0.25

bd: below detection limit; -: not analyzed. R, M, and L denote right, middle, and left portions, respectively. M_D denotes dark glass in the middle portion (see Fig. 5a).

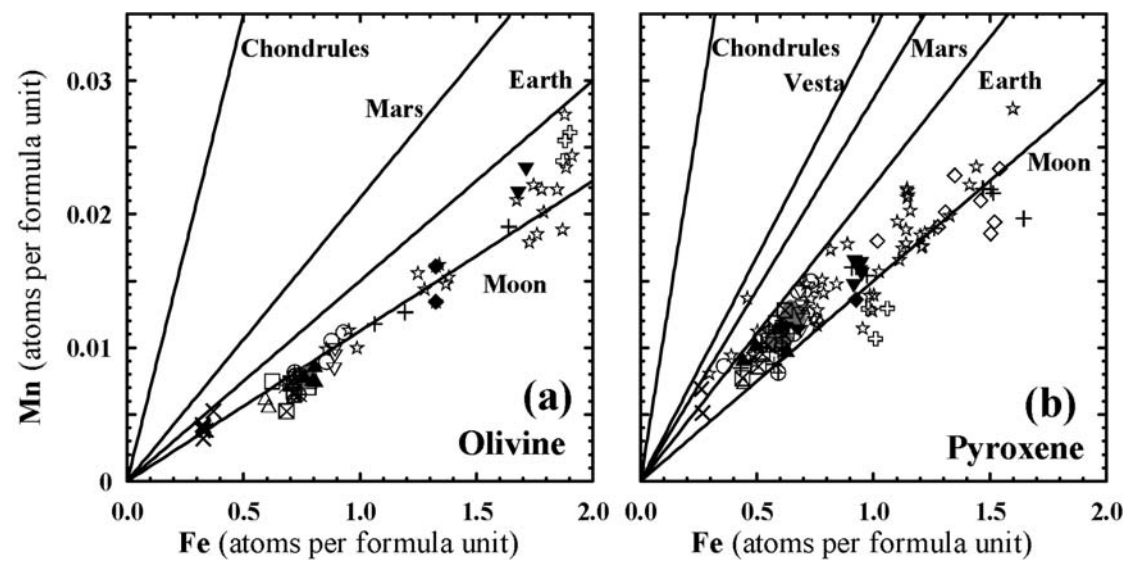


Fig. 8. Fe-Mn ratios in Dhofar 1180 for (a) olivine and (b) pyroxene compared to typical planetary fractionation trends complied by Papike et al. (2003). Atoms per formula unit are based on 4 oxygen atoms for olivine and 6 oxygen atoms for pyroxene. Legends are the same as those in Fig. 7.

Table 9. Bulk compositions (ppm) of Dhofar 1180 and comparison with other lunar meteorites.

	-			Calcalong	SaU 300	Yamato			
		Dhofar 118	30	Creek	INAA	793274	QUE 94281	EET 96008	
	Thi	s study	Korotev	Hill and	Hsu et al.	Koeberl et al.	Jolliff et al.	Anand et al.	
	INAA	s.d.	et al. (2008)	Boynton (2003)	(2008)	(1991)	(1998)	(2003)	
Fe (wt%)	4.91	0.046	7.17	7.53	6.20	11.8	10.27		
Sc	15.53	0.16	26.8	21.24	18.9	31.9	28.4	45.4	
Cr	869	9	1040	1170	1450	2010	1764	2530	
Co	15.68	0.16		24.82	38	41.4	45.3		
Ni	112	10	130	180	465	100	300		
Br	0.42	0.18		0.829	0.67	0.21			
Sr	1973	20		149.2		100	119	112.4	
Zr	47	10		354	50	81	100	112	
Cs	0.052	0.019		0.367	< 0.08	0.1	0.09	0.06	
Ba	594	8		257	54	97	78	80.2	
La	4.18	0.04		21.83	2.50	7	6.77	7.3	
Ce	10.67	0.14		54.1	6.1	17.9	18.1	19.7	
Nd	6.7	0.9		29.5	3.88	12	10	12.7	
Sm	2.140	0.02	2.84	9.55	1.11	3.56	3.21	3.65	
Eu	0.856	0.01	0.899	1.303	0.64	0.96	0.85	0.9	
Tb	0.453	0.011		1.941	0.24	0.76	0.68	0.79	
Yb	1.711	0.018		7.5	1.30	2.73	2.45	2.86	
Lu	0.239	0.003		1.024	0.17	0.376	0.342	0.42	
Hf	1.55	0.03		7.15	0.90	2.96	2.54	2.42	
Ta	0.213	0.009		0.991	0.108	0.34	0.33	0.34	
W	<1.6			0.554	0.19		0.18		
Ir (ppb)	3.6	0.6		3	19	6.2	10.5		
Au (ppb)	10.1	1.2		3	7	3	2.8		
Th	0.696	0.017	0.90	4.28	0.45	1.05	1.04	0.82	
U	0.37	0.06		1.18	0.22	0.26	0.27	0.3	

(1996) proposed an approach to estimate bulk TiO_2 contents of parental basalts from Ti# in pyroxenes at Fe#=0.5. Using this approach, the estimated TiO_2 contents are within \pm 20% of the measured bulk TiO_2 contents (Arai et al. 1996; Anand

et al. 2003). According to the correlation between Fe# and Ti# in pyroxene grains from mare lithic clasts in Dhofar 1180, an average Ti# value at Fe# = 0.5 is about 0.7 (Fig. 11). The estimated bulk TiO_2 content is about 2.7 wt% (Fig. 12). This

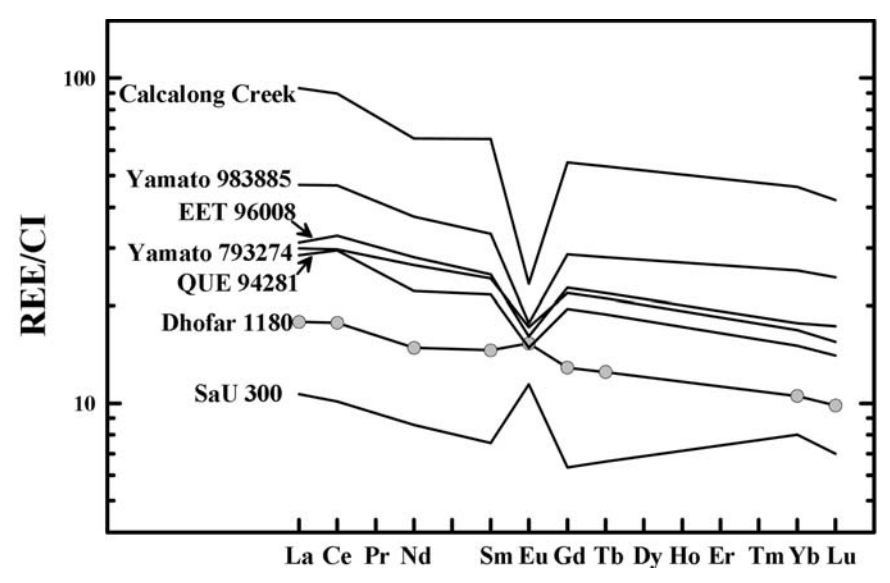


Fig. 9. CI-normalized (Anders and Grevesse 1989) REE abundances of Dhofar 1180 and some lunar meteorites. Data are from Koeberl et al. (1991); Jolliff et al. (1998); Anand et al. 2003; Hill and Boynton (2003), Karouji et al. (2006), and Hsu et al. (2008).

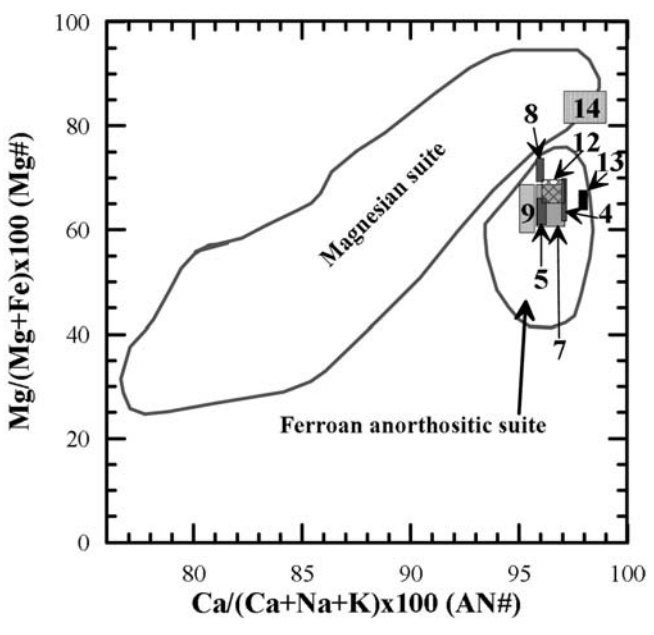


Fig. 10. Mg# of mafic phases (olivine and pyroxenes) versus AN# of coexisting plagioclase in lithic clasts of Dhofar 1180 and comparison with ferroan anorthositic suite and magnesian suite rocks. Regions of ferroan anorthositic suite and magnesian suite rocks are adopted from Lucey et al. (2006).

value is within the range of low-Ti mare basalts. Thus, mare lithic clasts in Dhofar 1180 have a strong affinity to low-Ti mare basalts.

Impact Origin and Chemical Diversity of Glasses

Glasses are a common component in lunar soils. There are two processes that produce lunar glasses: impact melting (impact origin) and pyroclastic eruption (volcanic origin).

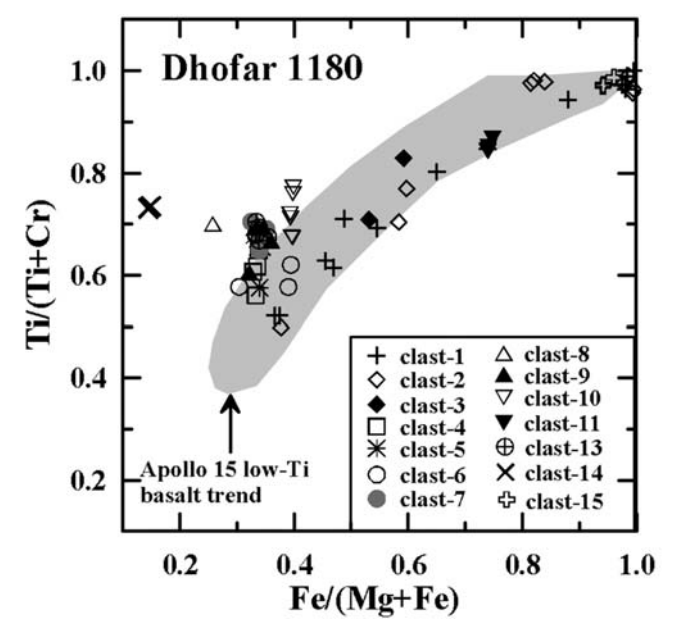


Fig. 11. Fe/[Mg+Fe] versus Ti/[Ti+Cr] for pyroxene of lithic clasts in Dhofar 1180. Shadowed area of Apollo 15 low-Ti basalt trend is adopted from Joy et al. (2006).

Delano (1986) proposed several criteria to distinguish glasses of volcanic origin from impact origin. Volcanic glasses contain no exotic mineral and/or lithic inclusions. They are homogeneous within individual samples and have crystal/liquid fractionation trends among different samples. They also have high Mg/Al ratio compared to multi-component lunar regolith and have uniform, Mg-correlated Ni abundances (Delano 1986). In addition, most volcanic glasses typically occur as glassy spherules (Zeigler et al. 2006). In Dhofar 1180, most glasses have irregular shapes. Only one has a sub-rounded shape; however, this glass is heterogeneous

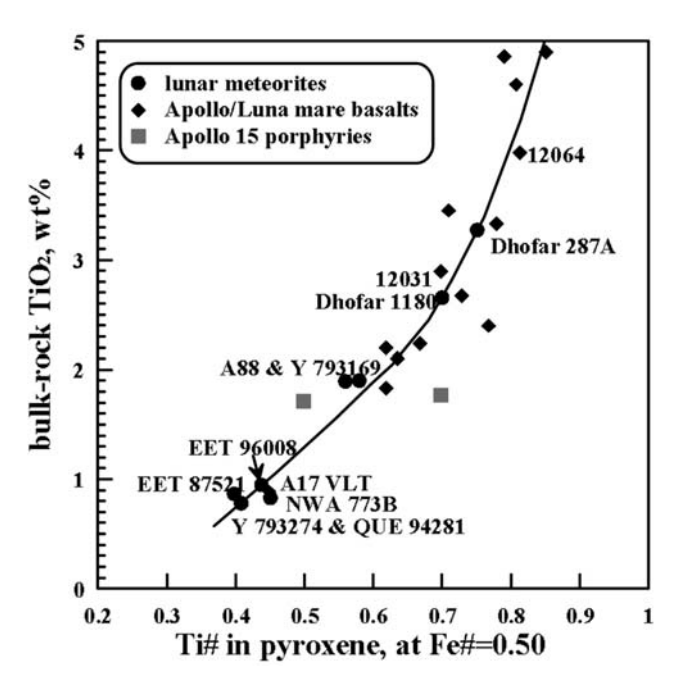


Fig. 12. Fe# normalized Ti# of pyroxene versus bulk TiO_2 content for low-Ti and very low-Ti mare basalts. The line is the correlation curve adopted from Anand et al. (2003). Data are from Arai et al. (1996), Arai and Warren (1999), and Anand et al. (2003).

and contains relict pyroxene grain and coexists with plagioclase glass. Most glasses contain mineral inclusions (even very fine-grained FeNi-metal, Figs. 4b and 4d) and have low MgO content. The mafic glasses free of mineral inclusions also have low MgO/Al₂O₃ ratios distinct from the range of known volcanic glasses (c.f. Zeigler et al. 2006). Thus, glasses in Dhofar 1180 are probably not of volcanic origin but most likely a product of impact.

Although impacts could cause melting of target materials, most impact glasses are considered as products of small impacts. Large impacts (e.g., massive basinforming impacts) could cause melting of all target materials; at the same time, high energies companying with large impacts usually produce crystalline impact melt breccias rather than glasses. In addition, Delano (1991) suggested that lunar impact glasses represent compositions of regolith rather than rocks (single lithology). This interpretation has been accepted by recent investigations (e.g., Taylor et al. 2003; Zeigler et al. 2006). Thus, diverse glasses represent various target materials, possibly indicating different impact craters (e.g., mafic glasses in Apollo 16 soils, Zeigler et al. 2006).

In Dhofar 1180, glasses occur with various petrographic and chemical features. Mafic glasses containing mineral inclusions also have several weight percents of Al₂O₃. This indicates that these glasses formed by melting of precursor materials containing plagioclase. High FeO contents and low Mg# values of the glasses indicate that they represent glasses from mare regions. Further, on the basis of their low to intermediate TiO₂ contents, it can be inferred that these

glasses probably originated from regions containing low-Ti mare basalts. However, major element compositions of the glasses are different from known low-Ti mare basalts, indicating that these glasses do not represent single lithology of known mare basalts. In addition, although trace-element compositions are unavailable in this study, some of these glasses also have high P_2O_5 contents and moderate K_2O contents. This probably indicates that these glasses contain various amounts of a KREEPy component.

Two groups of glasses free of mineral inclusions have different chemical compositions. Group-1 glasses have major-element compositions very similar to the KREEPy glass in Apollo 16 soils (Table 2 of Zeigler et al. 2006). Furthermore, their Mg# values are also close to each other. The similarity of these glasses to KREEPy glass suggests that the group-1 mafic glasses represent a KREEPy component in Dhofar 1180. On the CaO/Al₂O₃ versus MgO/Al₂O₃ diagram, these data also plot in the region of incompatible-element-rich glasses (Fig. 13a). The moderate K₂O contents also support this conclusion (Fig. 13b). Group-2 glasses are slightly different in major-element compositions from Group-1 glasses; however, the Mg# values, K₂O and P₂O₅ contents of the two group glasses are distinctly different. The low K₂O and P₂O₅ contents probably suggest that Group-2 glasses contain no KREEPy component, more likely representing mare-highlands glasses (Fig. 13).

Feldspathic glasses free of mineral inclusions are similar in major-element compositions to some Apollo 16 glasses (Papike et al. 1998). However, their Mg# values (0.52–0.54) are lower than those of Apollo 16 glasses (>0.59). Furthermore, these glasses are different from known highlands feldspathic rocks, indicating that they do not represent a single lithology. They probably are mixture of anorthosite and some Fe-rich phases. The relatively high TiO₂ contents which are distinct from anorthosite or anorthositic glasses in Apollo samples and other lunar meteorites also support this conclusion. Feldspathic glasses containing mineral inclusions have major-element compositions very close to anorthite, indicating melting of anorthite by impacts.

The vermiform texture of the P-rich glass (Fig. 5a) indicates silicate liquid immiscibility. Silicate liquid immiscibility has been used to explain separation of Fe-rich mineral assemblage and Si-rich mineral assemblage in Apollo and Luna samples (e.g., Apollo 15 KREEP, Hollister and Crawford 1977; the Luna 16 core sample, Roedder and Weiblen 1972). However, their petrographic textures are different from that of the P-rich glass in Dhofar 1180. The texture of the P-rich glass in Dhofar 1180 is probably the first direct evidence of Fe-rich and Si-rich liquid immiscibility. In addition, the high contents of K₂O, P₂O₅, and some trace elements (e.g., La, Th, Y, and Ce) indicate that the P-rich glass is closely related to KREEPy component. The P-rich glass has low Mg# values (0.23–0.26), probably representing residual melt of a highly fractionated mare basalt. However, the textural variation in a 20 µm scale (Fig. 5a) could not be

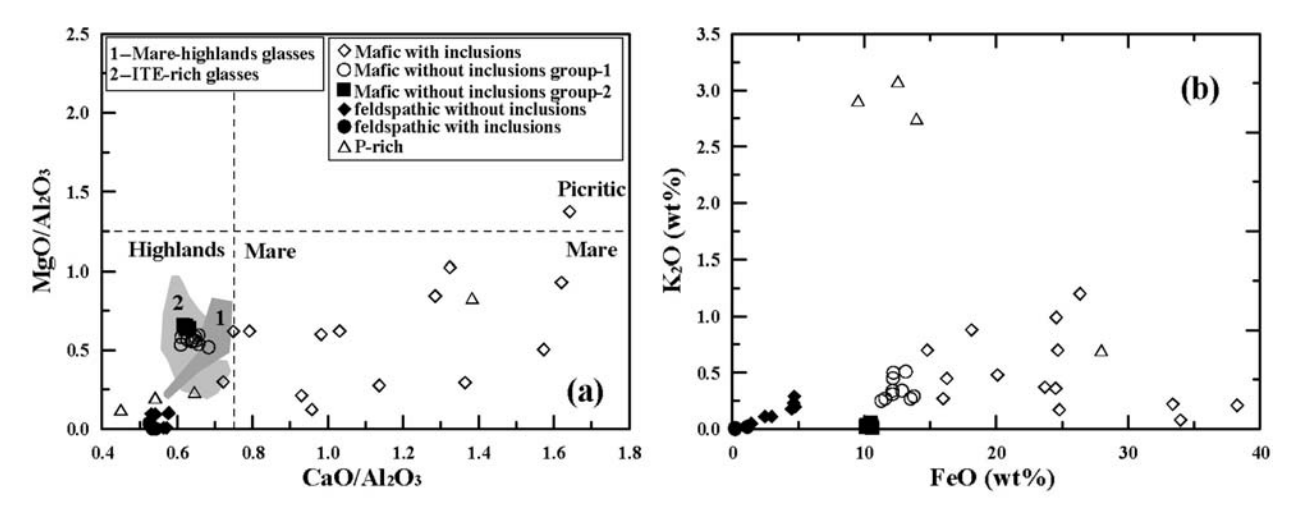


Fig. 13. Chemical composition of glasses in Dhofar 1180. a) The major element ratios CaO/Al₂O₃ and MgO/Al₂O₃ distinguish between highlands, mare, and picritic glasses. The dashed lines highlight the ratios of CaO/Al₂O₃ and MgO/Al₂O₃ and shadowed regions are adopted from Zeigler et al. (2006). b) K₂O versus FeO concentrations in different glasses.

explained by fractionation crystallization; instead, it could be caused by shock melting. Shock caused the melting of the precursor of the P-rich glass. When temperature decreased, the rim cooled rapidly and some spherule glasses formed; whereas the center cooled relatively slowly and vermiform texture formed.

Comparison with Other Lunar Rocks and Implications

Dhofar 1180 is a polymict lunar regolith breccia containing not only highlands feldspathic components but also Fe-rich mare components. Lithic clasts and glasses representing highly fractionated rocks or their residual melts are also present in this meteorite. These features indicate that Dhofar 1180 is one of mingled lunar breccias. Thus, we compare Dhofar 1180 mainly with other mingled lunar breccias and discuss its implication. It should be noted that concentrations of some elements (e.g., Fe, Sc, Cr, Ni, Sm, Eu, and Th) of our Dhofar 1180 sample are systematically lower than those reported by other others (e.g., Bunch et al. 2006; Korotev et al. 2008).

Apollo 16 is the only mission that landed in a highlands region of the lunar nearside. Similar to Dhofar 1180, Apollo 16 soils contain both highlands and mare components. However, numerous differences exist between Dhofar 1180 and Apollo 16 soils. First, KREEP-related glasses were found in Apollo 16 soils (e.g., Delano 1991; Zeigler et al. 2006; Delano et al. 2007), whereas Dhofar 1180 do not contain KREEP components. Second, glasses between Dhofar 1180 and Apollo 16 soils have various population and chemical compositions. For instance, glasses in Dhofar 1180 are mainly of impact origin whereas volcanic glasses also exist in Apollo 16 soils, although the amount is small. These differences suggest Dhofar 1180 is distinct from Apollo 16 soils.

Dhofar 1180 has a bulk Al₂O₃ content (22.6 wt%, Bunch et al. 2006) similar to that of Y-983885, Calcalong Creek (Bunch et al. 2006; Korotev et al. 2008) and SaU 300 (Hsu et al. 2008). In Y-983885, KREEP component occurs as a basalt clast (Arai et al. 2005). Calcalong Creek contains KREEP components; but lithic clasts with KREEP compositions were not observed (Hill and Boynton 2003). Hill and Boynton (2003) suggested that the KREEP carrier was in the melted matrix rather than in discrete clasts. Mare and KREEP components were not observed in SaU 300 (Hsu et al. 2008). Our studies show that Dhofar 1180 contains highlands and mare lithic clast and glasses, but no KREEP components were observed. Although some KREEPy lithic clasts and glasses were observed in Dhofar 1180, they could represent the latest phases in highly fractionated mare basalts and are different in petrography and mineral chemistry from KREEP components in Y-983885 and Calcalong Creek. REE abundance and pattern of Dhofar 1180 are distinctly different from those of Y-983885, Calcalong Creek, and SaU 300 (Fig. 9). REE abundances of Y-983885 and Calcalong Creek are significantly higher than those of Dhofar 1180 and the former two have a negative Eu anomaly (Fig. 9). SaU 300 has lower REE abundances and a larger positive Eu anomaly than Dhofar 1180 (Hsu et al. 2008).

Dhofar 1180 also differs from SaU 300, Y-983885, and Calcalong Creek in petrographic and mineralogical features. Glasses are more abundant in Dhofar 1180 than in SaU 300, Y-983885, and Calcalong Creek. In Dhofar 1180, mafic silicate minerals in mare lithic clasts and some mafic silicate mineral fragments are moderately to extremely Fe-rich. Both fayalite and pyroxferroite are present in Dhofar 1180. Mare pyroxenes show a Ti#-Fe# correlation trend similar to that of Apollo 15 low-Ti basalt trend. Mafic minerals in SaU 300 are moderately to highly rich in Mg (Mg# = 0.55–0.82) (Hsu et al. 2008). In Y-983885, most mafic minerals are Mg-rich with

Mg# of 0.66-0.77 (Arai et al. 2005). Fe-rich mafic grains are rather rare. Mafic minerals in Calcalong Creek are also Mgricher than those of Dhofar 1180 (Hill and Boynton 2003). There are several other mingled lunar breccias, such as EET 96008 (Anand et al. 2003), Y-793274 (Koeberl et al. 1991; Arai and Warren 1999), and QUE 94281 (Jolliff et al. 1998). Compared to these lunar breccias, Dhofar 1180 contains higher Al₂O₃ content and lower FeO content, implying a lower mafic component. In Fig. 9, EET 96008, Y-793274, and QUE 94281 have higher concentrations of rare-earth elements than Dhofar 1180. Distinctly, the former three mingled breccias have a negative Eu anomaly. In addition, mafic lithic clasts in these mingled breccias have a strong affinity to very-low-Ti basalts (Koeberl et al. 1991; Jolliff et al. 1998; Arai and Warren 1999; Anand et al. 2003); however, mafic lithic clasts in Dhofar 1180 have a strong affinity to low-Ti basalts. This distinction indicates mafic lithic clasts in Dhofar 1180 have difference source region from those in EET 96008, Y-793274, and QUE 94281. In summary, Dhofar 1180 has different petrologic, mineralogical, and chemical features compared to other known lunar rocks and represents a unique lunar breccia that has not been sampled in Apollo and Luna missions and other meteorites.

The remote sensing data from Clementine and Lunar Prospector reveal that the far side of the Moon is composed almost exclusively of highlands terrains with little mare and KREEP components and that the nearside is dominated by feldspathic highlands, mare, and KREEP rocks (Jolliff et al. 2000). Especially, extremely high-Fe rocks exclusively occur in the nearside (Jolliff et al. 2000). The fact that both feldspathic highlands clasts and extremely Fe-rich basaltic clasts occur in Dhofar 1180 might suggest that this meteorite could have been derived from the lunar nearside rather than the far side. Haskin (1998) established a relationship between Th distribution at the lunar highlands surface and distance from the center of Imbrium Basin. Th concentration decreases from the edge of Imbrium basin (~5 ppm) to a distance of ~4000 km (<1 ppm). This relationship is generally consistent with the Lunar Prospector gamma-ray data (Lawrence et al. 1998). Th concentration in Dhofar 1180 is relatively low [0.9 ppm, Bunch et al. (2006) and 0.7 ppm of this study] and no KREEP components were observed. This indicates that Dhofar 1180 is probably derived from an area at a great distance far from the center of the Imbrium Basin.

Acknowledgments—The authors thank Dr. Randy L. Korotev for performing INAA of Dhofar 1180. The critical and constructive reviews by Drs. Tomoko Arai, Beda Hofmann, Mahesh Anand, and Associate Editor Christian Koeberl, are greatly appreciated. The first author is benefited from the discussion with Prof. Lawrence A. Taylor. This work was supported by the Natural Science Foundation of China (Grant Nos. 40773046, 40703015, and 10621303), the Minor Planet

Foundation of China, and the Open Foundation of State Key Laboratory for Mineral Deposits Research, Nanjing University (Grant No. 14-8-6).

Editorial Handling-Dr. Christian Koeberl

REFERENCES

- Al-Kathiri A., Gnos E., and Hofmann B. A. 2007. The regolith portion of the lunar meteorite Sayh al Uhaymir 169. *Meteoritics & Planetary Science* 42:2137–2152.
- Anand M., Taylor L. A., Neal C. R., Snyder G. A., Patchen A., Sano Y., and Terada K. 2003. Petrogenesis of lunar meteorite EET 96008. Geochimica et Cosmochimica Acta 67:3499–3518.
- Anders E. and Grevesse N. 1989. Abundances of the elements: Meteoritic and solar. Geochimica et Cosmochimica Acta 53:197–214.
- Arai T., Otsuki M., Ishii T., Mikouchi T., and Miyamoto M. 2005. Mineralogy of Yamato 983885 lunar polymict breccia with a KREEP basalt, a high-Al basalt, a very low-Ti basalt and Mg-rich rocks. Antarctic Meteorite Research 18:17–45.
- Arai T., Takeda H., and Warren P. H. 1996. Four lunar mare meteorites: Crystallization trends of pyroxene and spinels. *Meteoritics & Planetary Science* 31:877–892.
- Arai T. and Warren P. H. 1999. Lunar meteorite Queen Alexandra Range 94281: Glass compositions and other evidence for lauch pairing with Yamato 793274. *Meteoritics & Planetary Science* 34:209–234.
- Bunch T. E., Wittke J. H., and Korotev R. L. 2006. Petrology and composition of lunar feldspathic breccias NWA 2995, Dhofar 1180 and Dhofar 1428. Meteoritics & Planetary Science 41:A31.
- Cahill J. T., Floss C., Anand M., Taylor L. A., Nazarov M. A., and Cohen B. A. 2004. Petrogenesis of lunar highlands meteorites: Dhofar 025, Dhofar 081, Dar al Gani 262, and Dar al Gani 400. Meteoritics & Planetary Science 39:503–529.
- Delano J. W. 1986. Pristine lunar glasses: criteria, data, and implications. *Journal of Geophysical Research* 91:D201–D213.
- Delano J. W. 1991. Geochemical comparison of impact glasses from lunar meteorites ALHA81005 and MAC 88105 and Apollo 16 regolith 64001. Geochimica et Cosmochimica Acta 55:3019– 3029.
- Delano J. W., Zellner N. E. B., Barra F., Olson E., Swindle T. D., Tibbetts N. J., and Whittet D. C. B. 2007. An integrated approach to understanding Apollo 16 impact glasses: Chemistry, isotopes, and shape. *Meteoritics & Planetary Science* 42:993– 1004.
- Fagan T. J., Taylor G. J., Keil K., Hicks T. L., Killgore M., Bunch T. E., Wittke J. H., Mittlefehldt D. W., Clayton R. N., Mayeda T. K., Eugster O., Lorenzetti S., and Norman M. D. 2003. Northwest Africa 773: Lunar origin and iron-enrichment trend. *Meteoritics & Planetary Science* 38:529–554.
- Gnos E., Hofmann B. A., Al-Kathiri A., Lorenzetti S., Eugster O., Whitehouse M. J., Villa I., Jull A. J. T., Eikenberg J., Spettel B., Krähenbühl U., Franchi I. A., and Greenwood G. C. 2004. Pinpointing the source of a lunar meteorite: Implications for the evolution of the Moon. *Science* 305:657–659.
- Haskin L. A. 1998. The Imbrium impact event and the thorium distribution at the lunar highlands surface. *Journal of Geophysical Research* 103:1679–1689.
- Hill D. H. and Boynton W. V. 2003. Chemistry of the Calcalong Creek lunar meteorite and its relationship to lunar terranes. *Meteoritics & Planetary Science* 38:595–626.
- Hollister L. S. and Crawford M. L. 1977. Melt immiscibility in

- Apollo 15 KREEP: Origin of Fe-rich mare basalts. Proceedings, 8th Lunar Science Conference. pp. 2419–2432.
- Hsu W., Zhang A., Bartoschewitz R., Guan Y., Ushikubo T., Krähenbühl U., Niedergesaess R., Pepelnik R., Reus U., Kurtz T., and Kurtz P. 2008. Petrography, mineralogy, and geochemistry of lunar meteorite Sayh al Uhaymir 300. *Meteoritics & Planetary Science* 43:1363–1381.
- Jolliff B. L., Korotev R. L., and Rockow K. M. 1998. Geochemistry and petrology of lunar meteorite Queen Alexandra Range 94281, a mixed mare and highland regolith breccia, with special emphasis on very-low-titanium mafic components. *Meteoritics & Planetary Science* 33:581–601.
- Jolliff B. L., Gillis J. J., Haskin L. A., Korotev R. L., and Wieczorek M. A. 2000. Major lunar crustal terranes: Surface expressions and crustal-mantle origins. *Journal of Geophysical Research* 105:4197–4216.
- Joy K. H., Crawford I. A., Downes H., Russell S. S., and Kearsley A. T. 2006. A petrological, mineralogical, and chemical analysis of the lunar mare basalt meteorite LaPaz Icefield 02205, 02224, and 02226. Meteoritics & Planetary Science 41: 1003–1025
- Joy K. H., Fernandes V. A., Burgess R., Crawford I. A., Irving A. J., and Kearsley A. T. 2007. The clast inventory of KREEPy lunar meteorite Northwest Africa 4472 (abstract #5223). *Meteoritics & Planetary Science* 42:A79.
- Karouji Y., Arai T., and Ebihara M. 2006. Chemical composition of another KREEP-rich lunar regolith breccia Yamato 983885 (abstract #1919). 37th Lunar and Planetary Science Conference. CD-ROM.
- Koeberl C., Kurat G., and Brandstätter F. 1991. Lunar meteorite Yamato-793274: mixture of mare and highland components, and barringerite from the Moon. *Proceedings of the NIPR Symposium on Antarctic Meteorites* 4:33–55.
- Koeberl C., Kurat G., and Brandstätter F. 1996. Mineralogy and geochemistry of lunar meteorite Queen Alexandra Range 93069. *Meteoritics & Planetary Science* 31:897–908.
- Korotev R. L. 1991. Geochemical stratigraphy of two regolith cores from the central highlands of the Moon. Proceedings, 21st Lunar and Planetary Science Conference. pp. 229–289.
- Korotev R. L. 1996. A self-consistent compilation of elemental concentration data for 93 geochemical reference samples. *Geostandards Newsletter* 20:217–245.
- Korotev R. L. 2005. Lunar geochemistry as told by lunar meteorites. *Chemie der Erde* 65:297–346.
- Korotev R. L., Irving A. J., and Bunch T. E. 2008. Keeping up with the lunar meteorites—2008 (abstract #1209). 39th Lunar and Planetary Science Conference. CD-ROM.
- Lawrence D. J., Feldman W. C., Barraclough B. L., Binder A. B., Elphic R. C., Maurice S., and Thomsen D. R. 1998. Global elemental maps of the Moon: The Lunar Prospector gamma-ray spectrometer. *Science* 281:1484–1489.
- Lindsley D. H., Papike J. J., and Bence A. E. 1972. Pyroxferroite: Breakdown at low pressure and high temperature. 3rd Lunar Science Conference. pp. 483–485.
- Liu Y., Floss C., Day J. M. D., Hill E., and Taylor L. A. 2009. Petrogenesis of lunar mare basalt meteorite Miller Range 05035. Meteoritics & Planetary Science 44:261–284.
- Lucey P., Korotev R. L., Gillis J. J., Taylor L. A., Lawrence D.,

- Campbell B. A., Elphic R., Feldman B., Hood L. L., Hunten D., Mendillo M., Noble S., Papike J. J., Reedy R. C., Lawson S., Prettyman T., Gasnault O., and Maurice S. 2006. Understanding the lunar surface and space-Moon interactions. In *New views of the Moon*, edited by Jolliff B. L., Wieczorek M. A., Shearer C. K., and Neal C. R. Reviews in Mineralogy & Geochemistry, vol. 60. Washington, D. C.: Mineralogical Society of America. pp. 83–219.
- Nielsen R. J. and Drake M. J. 1978. The case for at least three mare basalt magmas at the Luna 24 landing site. In *Mare Crisium: The view from Luna* 24, edited by Merrill R. B. and Papike J. J. New York: Pergamon. 419–428.
- Palme H., Spettel B., Jochum K. P., Dreibus G., Weber H., Weckwerth G., Wänke H., Bischoff A., and Stöffler D. 1991. Lunar highland meteorites and the composition of the lunar crust. *Geochimica et Cosmochimica Acta* 55:3105–3122.
- Papike J. J. 1998. Comparative planetary mineralogy: Chemistry of melt-derived pyroxene, feldspar, and olivine. In *Planetary materials*, edited by Papike J. J. Reviews in Mineralogy & Geochemistry, vol. 36. Washington, D.C.: Mineralogical Society of America. pp. 7.1–7.11.
- Papike J. J., Karner J. M., and Shearer C. K. 2003. Determination of planetary basalt parentage: A simple technique using the electron microprobe. *American Mineralogist* 88:469–472.
- Papike J. J., Ryder G., and Shearer C. K. 1998. Lunar samples. In Planetary materials, edited by Papike J. J. Reviews in Mineralogy & Geochemistry, vol. 36. Washington, D.C.: Mineralogical Society of America. pp. 5.1–5.234.
- Roedder E. and Weiblen P. W. 1972. Silicate melt inclusions and glasses in the lunar soil fragments from the Luna 16 core sample. *Earth and Planetary Science Letters* 13:272–285.
- Takeda H., Yamaguchi A., Bogard D. D., Karouji Y., Ebihara M., Ohtake M., Saiki K., and Arai T. 2006. Magnesian anorthosites and a deep crustal rock from the farside crust of the moon. *Earth and Planetary Science Letters* 247:171–184.
- Taylor L. A., Pieters C., Patchen A., Taylor D. H., Morris R. V., Keller L. P., and McKay D. S. 2003. Mineralogical characterization of lunar highland soils (abstract #1774). 34th Lunar and Planetary Science Conference. CD-ROM.
- Treiman A. H. and Drake M. J. 1983. Origins of lunar meteorite ALHA81005: Clues from the presence of terrae clasts and a very low titanium basalts clast. *Geophysical Research Letters* 10:783– 786.
- Warren P. H. 1985. The magma ocean concept and lunar evolution. Annual Review of Earth and Planetary Sciences 13:201–240.
- Warren P. H. and Kallemeyn G. W. 1991. Geochemical investigation of five lunar meteorites: Implications for the composition, origin and evolution of the lunar crust. *Proceedings of the NIPR Symposium on Antarctic Meteorites* 4:91–117.
- Zeigler R. A., Korotev R. L., Jolliff B. L., Haskin L. A., and Floss C. 2006. The geochemistry and provenance of Apollo 16 mafic glasses. *Geochimica et Cosmochimica Acta* 70:6050–6067.
- Zhang A. and Hsu W. 2006. Petrographic and mineralogical studies of the lunar meteorite Dhofar 1180 (abstract). *Meteoritics & Planetary Science* 41:A197.
- Zhang A. and Hsu W. 2007. A KREEP clast in the lunar meteorite Dhofar 1180 (abstract #1108). 38th Lunar and Planetary Science Conference. CD-ROM.